

**PREPARATION OF TUNGSTEN OXIDE FROM  
SCHEELITE ORE FROM SAMOENG DISTRICT,  
CHIANG MAI PROVINCE**

**METHIYANUN SUEPKHAM**

**MASTER OF SCIENCE  
IN CHEMISTRY**

ลิขสิทธิ์มหาวิทยาลัยเชียงใหม่  
Copyright© by Chiang Mai University  
All rights reserved

**GRADUATE SCHOOL  
CHIANG MAI UNIVERSITY  
MARCH 2019**

**PREPARATION OF TUNGSTEN OXIDE FROM SCHEELITE ORE  
FROM SAMOENG DISTRICT, CHIANG MAI PROVINCE**

**METHIYANUN SUEPKHAM**

**A THESIS SUBMITTED TO CHIANG MAI UNIVERSITY IN PARTIAL  
FULFILLMENT OF THE REQUIREMENTS FOR THE DEGREE OF  
MASTER OF SCIENCE  
IN CHEMISTRY**

**GRADUATE SCHOOL, CHIANG MAI UNIVERSITY  
MARCH 2019**

**PREPARATION OF TUNGSTEN OXIDE FROM SCHEELITE ORE  
FROM SAMOENG DISTRICT, CHIANG MAI PROVINCE**

METHIYANUN SUEPKHAM


THIS THESIS HAS BEEN APPROVED TO BE A PARTIAL FULFILLMENT OF  
THE REQUIREMENTS FOR THE DEGREE OF  
MASTER OF SCIENCE  
IN CHEMISTRY

**Examination Committee:**

**Advisor:**

 ..... Chairman  
(Dr. Ponlayuth Sooksamiti)

 .....  
(Asst. Prof. Dr. Sukjit Kungwankunakorn)

 ..... Member  
(Asst. Prof. Dr. Chumni Sangphagdee)

 ..... Member  
(Asst. Prof. Dr. Sukjit Kungwankunakorn)

Copyright © by Chiang Mai University  
All rights reserved

28 March 2019

Copyright © by Chiang Mai University

## ACKNOWLEDGEMENT

I would like to express my sincere thanks to my thesis advisor, Asst. Prof. Dr. Sukjit Kangwankunakorn for her invaluable help, teaching and advice throughout the cause of the thesis.

I very much thankful to Dr. Ponlayuth Sooksamiti, scientist, senior professional level at Department of Primary Industries and Mines, Chiang Mai for his suggestion and providing the scheelite ores.

Gratefully thank to the Department of Chemistry, Faculty of Science, Chiang Mai University and Department of Primary Industries and Mines, Chiang Mai for research facilities.

Finally, I would also like to thank my parents and friends who helped me in various ways in my thesis.

Methiyanun Suepkham

ลิขสิทธิ์มหาวิทยาลัยเชียงใหม่  
Copyright© by Chiang Mai University  
All rights reserved

<b>Thesis Title</b>	Preparation of Tungsten Oxide from Scheelite Ore from Samoeng District, Chiang Mai Province
<b>Author</b>	Miss Methiyanun Suepkham
<b>Degree</b>	Master of Science (Chemistry)
<b>Advisor</b>	Asst. Prof. Dr. Sukjit Kungwankunakorn

## ABSTRACT

Tungsten oxide or tungsten trioxide is chemical compound which consists of transition metal tungsten and oxygen. This chemical compound is an intermediate in the preparation of tungsten powder from its ore such as scheelite and wolframite. Tungsten oxide is widely used in industry to manufacture tungstate for x-ray screen phosphor, fireproofing fabrics and gas sensor. Moreover, tungsten oxide is also used as a pigment in ceramic and paints. Bo Kaeo mine in Samoeng District, Chiang Mai, Thailand exports tungsten in the form of scheelite concentrate. In order to increase the value of export of tungsten, the process for preparation of tungsten oxide from Samoeng's scheelite ore was studied. The leaching of tungsten from shceelite concentrate using nitric acid and phosphoric acid as chelating agent was chosen for a part of this work because this method was simple, non-necessity of high temperature and low waste generation. In this study, process for preparation tungsten oxide from Samoeng's scheelite ore by applying central composite design (CCD) would be developed. Various parameters namely, concentration of  $\text{HNO}_3$ , leaching temperature, leaching time,  $\text{W/PO}_4^{3-}$  weight ratio, calcination temperature and calcination time were studied for optimum condition. However, three important parameters, which affect recovery of tungsten including concentration of  $\text{HNO}_3$ , leaching temperature and  $\text{W/PO}_4^{3-}$  weight ratio were chosen for study first by applying central composite design to model the experiment. The recovery of tungsten was analyzed by multiple linear regression (MLR) for assess the significance of concentration of nitric acid, leaching temperature

and  $W/PO_4^{3-}$  weight ratio on recovery of tungsten oxide. The results were indicated in form of response surface plots using response surface methodology (RSM). As presented in the response surface plots, the optimum leaching condition was concentration of nitric acid of 4.0 M,  $W/PO_4^{3-}$  weight ratio of 1.5:1 and leaching temperature of 90 °C. The optimum leaching condition was used for study on the effect of leaching time, calcination time and calcination temperature on recovery of tungsten oxide. The results indicated that the optimum leaching time was 120 minutes. However, the recovery of tungsten oxide was practically independent of calcination time and calcination temperature. The optimum calcination time and optimum calcination temperature were 30 minutes and 600 °C, respectively.

หัวข้อวิทยานิพนธ์	การเตรียมทั้งสเดนออกไซด์จากสินแร่ซีไลต์จาก อำเภอสะเมิง จังหวัดเชียงใหม่
ผู้เขียน	นางสาว เมธิญานันท์ สืบคำ
ปริญญา	วิทยาศาสตรมหาบัณฑิต (เคมี)
อาจารย์ที่ปรึกษา	ผศ.ดร. สุขจิตต์ กังวานคุณากร

## บทคัดย่อ

ทั้งสเดนออกไซด์ หรือทั้งสเดนไดรออกไซด์ เป็นสารประกอบทางเคมีซึ่งประกอบด้วยธาตุโลหะทั้งสเดนและออกซิเจน สารประกอบทางเคมีชนิดนี้เป็นสารมัธยันต์ในการเตรียมผงทั้งสเดนจากสินแร่ทั้งสเดน เช่น สินแร่ซีไลต์และสินแร่วุลแฟรมไมต์ ทั้งสเดนออกไซด์ถูกใช้อย่างแพร่หลายในอุตสาหกรรมเพื่อการผลิตทั้งสเดนสำหรับหน้าจออิเล็กทรอนิกส์ ฝ้ากันไฟ และแก๊สเซ็นเซอร์ นอกจากนี้ทั้งสเดนออกไซด์ยังถูกใช้เป็นเม็ดสีในเครื่องเซรามิกและภาวาด เหมืองบ่อแก้ว อำเภอสะเมิง จังหวัดเชียงใหม่ ประเทศไทย ได้มีการส่งออกทั้งสเดนในรูปของหัวแร่ซีไลต์ เพื่อเป็นการเพิ่มมูลค่าในการส่งออกทั้งสเดน กระบวนการในการเตรียมทั้งสเดนออกไซด์จากสินแร่ซีไลต์จากอำเภอสะเมิงจึงถูกศึกษา กระบวนการชะทั้งสเดนจากสินแร่ซีไลต์ด้วยกรดไนตริกและใช้กรดฟอสฟอริกเป็นสารคีเลตถูกเลือกให้เป็นส่วนหนึ่งของงานนี้เนื่องจากวิธีการนี้ง่าย ไม่ต้องการอุณหภูมิที่สูง และให้ของเสียน้อยในการศึกษาครั้งนี้กระบวนการเตรียมทั้งสเดนออกไซด์จากสินแร่ซีไลต์จากอำเภอสะเมิงโดยทำการประยุกต์ร่วมกับ เซนทรัล คอมโพสิต ดีไซน์ ถูกพัฒนา ตัวแปรต่างๆ ได้แก่ ความเข้มข้นของกรดไนตริก อุณหภูมิที่ใช้ในการชะ เวลาที่ใช้ในการชะ สัดส่วนน้ำหนักของ  $W/PO_4^{3-}$  อุณหภูมิที่ใช้ในการเผา และเวลาที่ใช้ในการเผาถูกศึกษาเพื่อหาสภาวะที่เหมาะสม อย่างไรก็ตาม มีสามตัวแปรที่สำคัญซึ่งส่งผลต่อการกลับคืนของทั้งสเดนออกไซด์ ประกอบด้วย ความเข้มข้นของกรดไนตริก อุณหภูมิที่ใช้ในการชะ และสัดส่วนน้ำหนักของ  $W/PO_4^{3-}$  ถูกเลือกเพื่อศึกษาก่อนโดยประยุกต์ใช้ เซนทรัล คอมโพสิต ดีไซน์ ในการออกแบบการทดลอง ค่าการกลับคืนของทั้งสเดนออกไซด์ ถูกวิเคราะห์โดยวิธีมัลติเพิล ลิเนียร์ รีเกรซชัน เพื่อประเมินความสำคัญของความเข้มข้นของกรดไนตริก อุณหภูมิที่ใช้ในการชะและสัดส่วนน้ำหนักของ  $W/PO_4^{3-}$  ต่อการกลับคืนของทั้งสเดนออกไซด์ ผลจากการวิเคราะห์ได้แสดงในรูปแบบของแผนพื้นที่ผิวตอบสนองโดยใช้เทคนิคเรสพอนส์ เซอร์เฟส เมทโธดอร์โดโลจี

ตามที่แสดงไว้ในแผนพื้นที่ผิวตอบสนองสถานะสำหรับการชะที่เหมาะสมคือความเข้มข้นของกรดไนตริกคือ 4.0 โมลาร์ สัดส่วนน้ำหนักของ  $\text{W/PO}_4^{3-}$  คือ 1.5:1 และอุณหภูมิที่ใช้ในการชะคือ 90 องศาเซลเซียส สถานะสำหรับการชะที่เหมาะสมถูกใช้เพื่อศึกษาผลของเวลาที่ใช้ในการชะ เวลาที่ใช้ในการเผาและอุณหภูมิที่ใช้ในการเผาคือการกลับคืนของทั้งสเดนออกไซด์ จากผลการทดลองพบว่าเวลาที่ใช้ในการชะที่เหมาะสมคือ 120 นาที อย่างไรก็ตามการกลับคืนของทั้งสเดนออกไซด์นั้นไม่ขึ้นกับเวลาที่ใช้ในการเผาและอุณหภูมิที่ใช้ในการเผา ซึ่งเวลาที่เหมาะสมในการเผาและอุณหภูมิที่เหมาะสมในการเผาคือ 30 นาที และ 600 องศาเซลเซียสตามลำดับ



ลิขสิทธิ์มหาวิทยาลัยเชียงใหม่  
Copyright© by Chiang Mai University  
All rights reserved



# CONTENTS

	Page
Acknowledgement	c
Abstract in English	d
Abstract in Thai	f
List of Tables	k
List of Figures	l
List of Abbreviations and Symbols	n
Chapter 1 Introduction	
1.1 Introduction	1
1.2 Tungsten Oxide	3
1.3 Scheelite	4
1.4 Extraction of Metal from Ores	5
1.5 Central Composite design	8
1.6 Multivariate Calibration	10
1.7 X-Ray Fluorescence Spectrometry	13
1.8 X- Ray Diffraction Spectrometry	16
1.9 Fourier Transform Infrared Spectrometry	17
1.10 Scanning Electron Microscope Equipped whit Energy-Dispersive X-ray Spectroscopy	20
1.11 Gravimetric Method	22
1.12 Literature Reviews for Tungsten Extraction from Scheelite and Composite Scheelite	23
1.13 Research Objectives	27

## Chapter 2 Experimental

2.1 Apparatus and Chemical	
2.1.1 Material	28
2.1.2 Apparatus	29
2.1.3 Chemicals	30
2.2 Method	
2.2.1 Scheelite Ore Beneficiation	30
2.2.2 Preparation of Tungsten Oxide	31
2.2.3 Design of Experiments for Leaching Tungsten from Scheelite Concentrates	32
2.2.4 Optimization of Leaching Time	33
2.2.5 Optimization of Calcination Temperature	33
2.2.6 Optimization of Calcination Time	33
2.2.7 Characterization Techniques	34

## Chapter 3 Results and Discussion

3.1 Central Composite Design	35
3.2 Effect of Leaching Time	44
3.3 Effect of Calcination Temperature	46
3.4 Effect of Calcination Time	51
3.5 Characterization	
3.5.1 X-Ray Diffraction	54
3.5.2 Fourier Transform Infrared Spectroscopy	55
3.5.3 Scanning Electron Microscopy Equipped with Energy-Dispersive X-Ray Spectroscopy	56

	Page
Chapter 4 Conclusion	58
References	60
Curriculum Vitae	67



ลิขสิทธิ์มหาวิทยาลัยเชียงใหม่  
 Copyright© by Chiang Mai University  
 All rights reserved

## LIST OF TABLES

	Page
Table 1.1 The properties of tungsten oxide	3
Table 1.2 The properties of scheelite ore	5
Table 2.1 The main chemical compositions of scheelite concentrate	29
Table 2.2 Coded and actual levels of input parameters from central composite design	32
Table 3.1 The effects of leaching conditions on weight, color and percent recovery product weight	36
Table 3.2 Percent recovery of products, means and standard deviations	40
Table 3.3 Comparison between predicted values of percent recovery of product and actual values of percent recovery of product	43
Table 3.4 Effects of leaching times on weight, color and percent recovery of tungsten oxide	45
Table 3.5 Effect of calcination temperature on weight, color and percent recovery of tungsten oxide	47
Table 3.6 The crystallite size of tungsten oxide with different calcination temperature	50
Table 3.7 Effect of calcination times on weight, color and percent recovery of tungsten oxide	52
Table 3.8 The crystallite size of tungsten oxide with different calcination time	54

## LIST OF FIGURES

	Page
Figure 1.1 Crystal structure of monoclinic tungsten oxide	4
Figure 1.2 Scheelite ore and scheelite ore under ultraviolet light	5
Figure 1.3 Central composite design with three factors, A, B and C	8
Figure 1.4 The Central composite circumscribed design for three factors	9
Figure 1.5 The central composite inscribed design for three factors	9
Figure 1.6 The central composite face centered design for three factors	10
Figure 1.7 Example response surface plot with two factors	12
Figure 1.8 The X-ray fluorescence process	13
Figure 1.9 The wavelength dispersive X-ray fluorescence spectrometer schematic	14
Figure 1.10 The energy dispersive X-ray fluorescence spectrometer schematic	15
Figure 1.11 The X-ray diffraction process	16
Figure 1.12 The X-ray diffraction spectrometer diagram	17
Figure 1.13 The diagram of electromagnetic spectrum	18
Figure 1.14 The diagram of The Fourier Transform Infrared spectrometer	19
Figure 1.15 The schematic of scanning electron microscope instrument	20
Figure 1.16 Scanning electron microscopy scheme	21
Figure 2.1 The X-ray diffraction pattern of scheelite concentrate sample and standard X-ray diffraction pattern of scheelite	28
Figure 2.2 Scheelite ore beneficiation process flow diagram	30
Figure 2.3 Flowchart of tungsten oxide preparation	31
Figure 3.1 Response surface plots	42

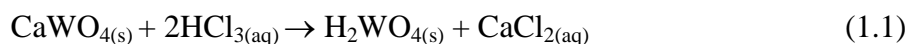
	Page
Figure 3.2 Effects of leaching time on percent recovery of tungsten oxide	44
Figure 3.3 Effects of calcination temperature on percent recovery of tungsten oxide	46
Figure 3.4 The X-ray diffraction pattern of product that obtained from calcination temperature of 500°C and standard X-ray diffraction pattern of tungstophosphoric acid	48
Figure 3.5 The X-ray diffraction pattern of tungsten oxide is obtained from calcination temperatures of 600, 700 and 800°C and standard X-ray diffraction pattern of tungsten oxide	49
Figure 3.6 Effects of calcination time on percent recovery of tungsten oxide	51
Figure 3.7 The X-ray diffraction pattern of tungsten oxide that obtained from calcination time of 30, 45 and 60 minutes and standard X-ray diffraction pattern of tungsten oxide	53
Figure 3.8 The X-ray diffraction pattern of tungsten oxide that was prepared under optimum condition and standard X-ray diffraction pattern of tungsten oxide	54
Figure 3.9 FTIR spectrum of tungsten oxide obtained by preparation under optimum condition.	55
Figure 3.10 Micrograph of the product obtained by preparation under optimum condition and micrograph of tungsten oxide	56
Figure 3.11 EDX elemental microanalysis analysis of product that was prepared under optimum condition.	57

# CHAPTER 1

## Introduction

### 1.1 Introduction

Tungsten oxide is the intermediate in the metallurgical industry, and being an important raw material for preparing tungsten powder from its ores such as scheelite and wolframite. Scheelite is an important ore of tungsten. This ore can be found with tin in Thailand. In northern Thailand, scheelite ores are found in Chiang Mai, Chiang Rai, Lampang, Tak, Mae Hong Son and Phrae. Bo Kaeo mine in Samoeng District, Chiang Mai, Thailand is the old tin and scheelite mine. At present, Bo Kaeo mine exports tungsten in the form of scheelite concentrate. To increase the value of tungsten export needs to prepare tungsten oxide from scheelite concentrate [1]. There are many methods for preparing tungsten oxide from scheelite concentrates. Generally, scheelite ores can be leached with sodium hydroxide or sodium carbonate at high temperature followed by solvent extraction or ion exchange to produce ammonium paratungstate crystalline. Ammonium paratungstate crystalline is calcinated under oxidizing condition at 500 to 700 °C to produce tungsten oxide. These methods are widely applied in the western countries. However, these methods require large amounts of reagent, high temperature and high pressure for obtaining high yield [2-3]. There are other methods to leach tungsten from scheelite concentrates for preparing tungsten. Hydrochloric acid leaching is one of conventional methods for leaching tungsten from scheelite concentrates. The reaction is expressed as:



However, all of the acidic leaching processes produce the solid film of tungstic acid ( $\text{H}_2\text{WO}_4$ ). The solid film of tungstic acid will cover the surface of unreacted scheelite particles and lead to low tungsten yield. In order to improve the leaching process

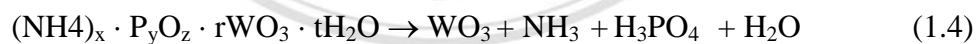
and obtain high yield of tungsten, the chelating agent that can form the water-soluble compound with tungsten is required. The chelating reagents, such as oxalic, phosphoric, tartaric, citric acid and any compounds containing  $\text{PO}_4^{3-}$  anion are used with acid for the avoidance of tungstic acid formation. Phosphoric acid and nitric acid were used to leach tungsten from Samoeng's scheelite concentrate for preparing tungsten oxide because nitric acid has provided advantages, such as less corrosive compare with hydrochloric acid and wastewater from leaching process can be treated into nitrogen fertilizer [4-5]. The leaching of tungsten from scheelite concentrate using nitric and phosphoric acid as chelating agent is represented by the following reaction:



As seen by the above reaction, tungsten is obtained in form of water-soluble phosphotungstic acid ( $\text{H}_3\text{PW}_{12}\text{O}_{40}$ ). Ammonium hydroxide is used for tungstate salt precipitation. The chemical reaction is as follows [4]:



The tungstate salt is calcined at the temperature equal to or greater than 600 °C to produce tungsten oxide ( $\text{WO}_3$ ). In the calcination process, tungstate salt is converted to tungsten oxide via the following reaction:



Many parameters were investigated in this research, such as nitric acid concentration, leaching temperature,  $\text{W}/\text{PO}_4^{3-}$  weight ratio, leaching time, calcination time and calcination temperature. However, the central composite design was used to model the experiments for leaching tungsten from Samoeng's scheelite concentrate and investigating effect of concentration of nitric acid, leaching temperature and  $\text{W}/\text{PO}_4^{3-}$  weight ratio on recovery of tungsten oxide. Central composite design is popular method for experimental design which corresponds to be one part of chemometric. This experiment design can investigate the interaction effects among parameters. Furthermore, central composite design requires smaller number of experiment compare to that of conventional experiment. The aims of this research are to prepare tungsten oxide from Samoeng's scheelite ore by applying central composition design (CCD) and



investigate the effects of parameters such as nitric acid concentrations, leaching temperatures, leaching time,  $W/PO_4^{3-}$  weight ratios, calcination temperatures and calcination times on the recovery of tungsten oxide [6].

## 1.2 Tungsten Oxide ( $WO_3$ )

Tungsten oxide also called tungsten trioxide is a chemical compound which consists of transition metal tungsten and oxygen. This chemical compound is insoluble in water and acid. However, it can be soluble in hot alkalis [2,7]. The properties of tungsten oxide are shown in Table 1.1.

**Table 1.1** The properties of tungsten oxide [3]

Properties	Tungsten oxide
Formula weight	231.838 g/mol
Melting point	1472 °C
Boiling point	1837 °C
density	7200 kg/m <sup>3</sup>

Tungsten oxide was first prepared in 1841 by Robert Oxland. It is an important precursor for the production of tungsten metal powder from its ore by heating with hydrogen at 850 °C. The most common tungsten ores are Wolfram and Scheelite. The isolation of tungsten is affected by the formation of tungstic acid. However, the chemical process chosen depends on the ore being used. In wolframite  $(Mn,Fe)WO_4$ , tungsten is converted to tungstate solution either by fusing with sodium hydroxide and leaching the cool product with water, or protracted boiling with aqueous alkalis. In scheelite  $(CaWO_4)$ , tungsten is converted to insoluble tungstic acid by direct treatment with hydrochloric acid and separated from the soluble salts of other metals. Tungstic acid is then roasted to tungsten oxide [2,8-9]. Crystalline structure of tungsten oxide depends on temperature. Normally, the structure of tungsten trioxide is monoclinic at 17 to 330 °C. There are other structures such as triclinic at -50 to 17 °C, orthorhombic at 330 to 740 °C and tetragonal at over 740 °C. Crystal structure of monoclinic tungsten oxide is shown in Figure 1.1, Tungsten oxide has four important types namely, yellow tungsten oxide ( $WO_3$ ), blue tungsten oxide ( $WO_{2.9}$ ), violet tungsten oxide ( $WO_{2.72}$  or

$W_{18}O_{49}$ ), and brown tungsten oxide ( $WO_2$ ). Tungsten oxide is important for various application, for example, used as a yellow pigment in ceramic glazes, used for textiles and in the plastic industry, used to produce tungstate for x-ray screens and fireproof fabrics as well as used to produce a translucent film for smart windows [2,10].

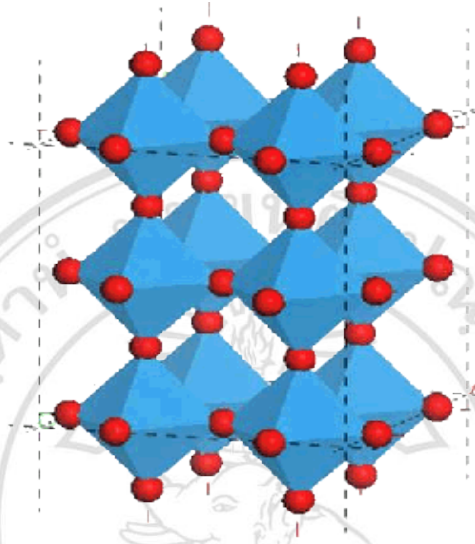


**Figure 1.1** Crystal structure of monoclinic tungsten oxide [11].

### 1.3 Scheelite ( $CaWO_4$ )

Scheelite is an important ore of tungsten. The chemical is  $CaWO_4$  containing CaO 19.4% and  $WO_3$  80.6%. Scheelite is named in honor of the Swedish chemist Karl Wilhelm Scheele, who determined the mineral contained tungsten. Scheelite commonly occurs as compact or granular masses in contact metasomatic deposits, high-temperature veins, and granite pegmatites. The properties of scheelite ore are shown in Table 1.2 [13-14].

**Table 1.2** The properties of scheelite ore [13-14]

Properties	Scheelite
Chemical formula	$\text{CaWO}_4$
Crystal system	Tetragonal
Hardness	4.5-5
Density	5.9-6.1 g/cm <sup>3</sup>
Refractive index	1.918-1.921
Colors	Colorless, white, gray, yellow, orange
Transparency	Transparent to opaque
Luster	Glassy to adamantine
Fluorescence	Blue under short wave ultraviolet light

Scheelite ore under normal light and scheelite ore under short wave ultraviolet light are shown in Figure 1.2.

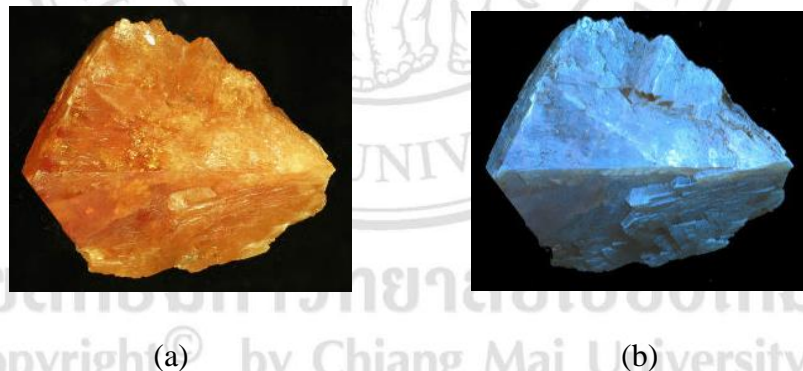


**Figure 1.2** (a) Scheelite ore under normal light; (b) Scheelite ore under short wave ultraviolet light [15].

#### 1.4 Extraction of Metals from Ores

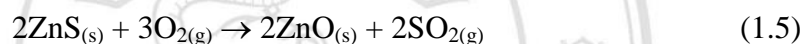
A metal ore is a rock containing metal or metal compound, in high enough concentration to make it economic to extract the metal. The type of process used to extract a metal from ore depends on the chemical nature of the mineral containing. However, the same metal can be produced often by several different methods. These

depend on economic considerations, the cost of raw materials and market conditions. There are three main processes of extracting metals from their ores [16-17].

### **1.4.1 Heating**

#### **1) Roasting**

Roasting is a metallurgical process which converts compounds to oxide. Typical ores usually roasted are the sulfide of lead, copper and zinc. This process involved in gas-solid reactions at elevated temperatures with the goal of purifying the metal component. Normally, roasting is carried out below the melting points of sulfides and oxides. Thus, the temperature range of interest is between 500 and 1000 °C. In this process, the ore is heated alone or mixed with other materials in the excess supply of air. The reaction is shown in the following equations.



During roasting, sulfide is converted to oxide, and sulfur is released as sulfur dioxide. This process is generally carried out in a furnace [17-18].

#### **2) Smelting**

Smelting is a metallurgical process of extracting metals from their ores at high temperatures. This process is widely used to extract metal from ore after mining. Smelting operations either process of oxidized ores or slags produced in other operations for the recovery of some metals. In this process, ore is mixed with reducing agent, such as coke, charcoal and silica. Then, ore is heated at high temperature beyond its melting point. During smelting, flux is added to the ore for removal of impurities. Flux combines with the impurity to produce a slag. The selection of flux depends on the impurities. For example, the smelting operations of iron are based on the use of coal as a reducing agent [17,19].



### 1.4.2 Leaching

Leaching is a chemical method for extracting metal from ores. There are many kinds of leaching process. To choose the most appropriate, it generally depends on the type of reagents that used for operation. The suitable reagent is selected according to the type of mineral being processed. The leaching processes can be carried out either in acid or in ammonia solutions, the latter being specifically suited to bring cobalt, nickel, and copper into solution as ammonia complexes. In this process, ore is dissolved in suitable reagent. The solution of ore is filtrated. Then, the ore is recovered by precipitation or crystallization. The advantages of leaching are simple and less harmful because its energy consumption is very low and gas pollution never occurs [17,20].

### 1.4.3 Electrolytic Reduction

The highly electropositive elements such as alkali metals and alkaline earth metals can be extracted from their ores by electrolysis of molten salt because these metals cannot be reduced using any of the above methods. The extraction of metal by the use of electrolysis is defined as the decomposition into ions of a chemical compound in solution by the action of an electric current passing through the solution. Electrolysis is the process of using electric current to induce a reduction-oxidation reaction. In this reaction, ion exchange their electrons and change oxidation state. For example, sodium metal is extracted by electrolysis of molten sodium chloride containing other salts as impurities.



During electrolysis, the cathode supplies electrons to metal ions for their reduction to the metal. However, the solubility of the metal in the electrolyte can be substantial with the possibility of re-oxidation at the anode. This reaction leads to obtain lower yield [19,21-22].

### 1.5 Central Composite Design (CCD)

Central composite design (CCD) or box Wilson design is a popular method for experimental design which corresponds to part of chemometric [23]. This method has three different design points, namely edge points, star points and center point. Edge points or factorial points are two-levels full factorial. Two-levels factorial ( $2^k$ ) is basic design which carry out all possible experiments with k factors, minimum and a maximum values [23-24]. Star points or axial points are the points in which all factors but one are set at the mid-value. The star points represent minimum and maximum values for each factor in the design. The center point is the response corresponding to the treatment exactly midway between the two values of all factors. This point is frequently useful to be able to estimate the experimental error. Therefore, one method is to perform extra replicates in center. Central composite design has 3 types which depend on where the star points placed, namely circumscribed (CCC), inscribed (CCI) and face centered (CCF) [25-28]. The central composite design is shown in Figure 1.3.

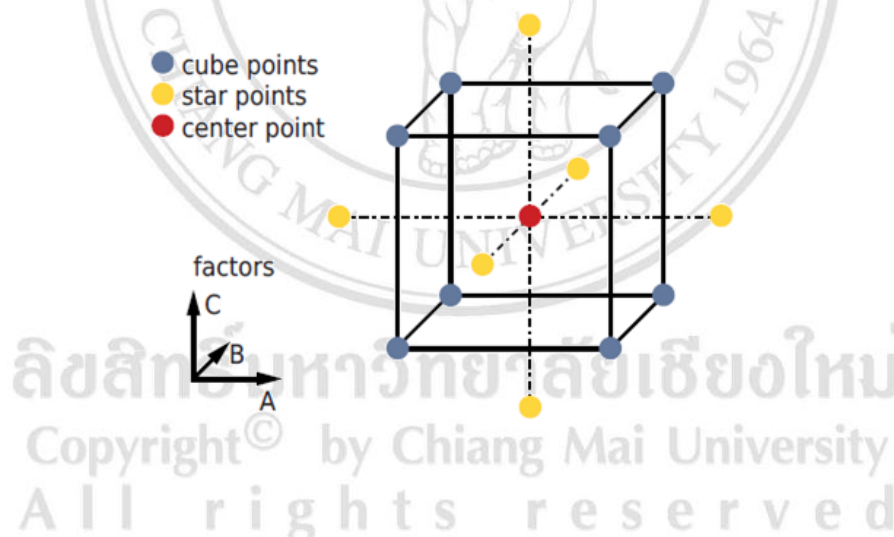


**Figure 1.3** The central composite design with three factors, A, B and C [29].

Central composite circumscribed (CCC) design is the original which central composite design. The Central composite circumscribed design for three factors is shown in Figure 1.4. The edge points are at the design limits. The star points are at some distance from the center depending on the number of factors in the design. The star points extend the range outside the minimum and maximum settings for all factors. The center points complete the design. Central composite circumscribed designs

provide high quality predictions over the entire design space. However, it must be certain that the star points remain at reasonable levels [24].

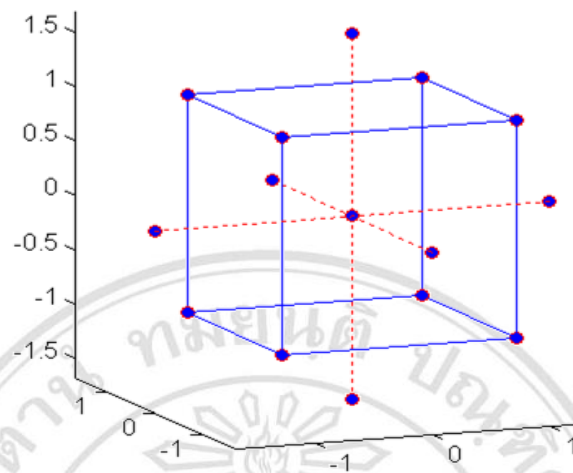


**Figure 1.4** The Central composite circumscribed (CCC) design for three factors [30].

In central composite inscribed (CCI) design, the star points are set at the design limits and the edge points are inside the range. The central composite inscribed design for three factors is shown in Figure 1.5. This design uses only points within the factor ranges originally specified and makes the prediction area is limited compared to the central composite circumscribed design [24].

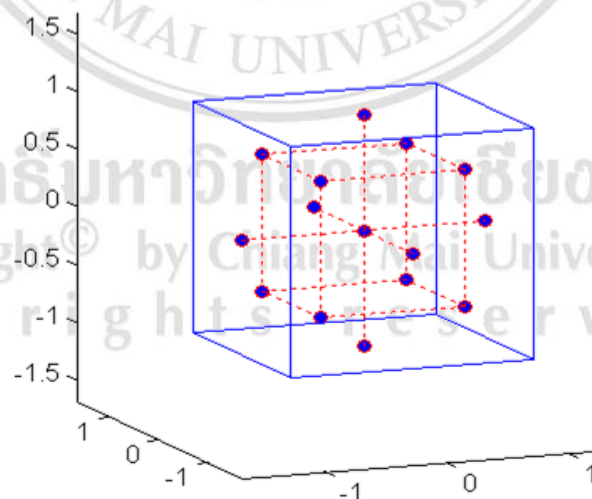


**Figure 1.5** The central composite inscribed (CCI) design for three factors [30].

In central composite face centered (CCF) design, the star points are at the center of each face of the factorial space. The central composite face centered design for three



factors is shown in Figure 1.6. This design provides relatively high quality predictions over the entire design range. However, central composite face centered design provides poor precision for estimating pure quadratic coefficients [30].

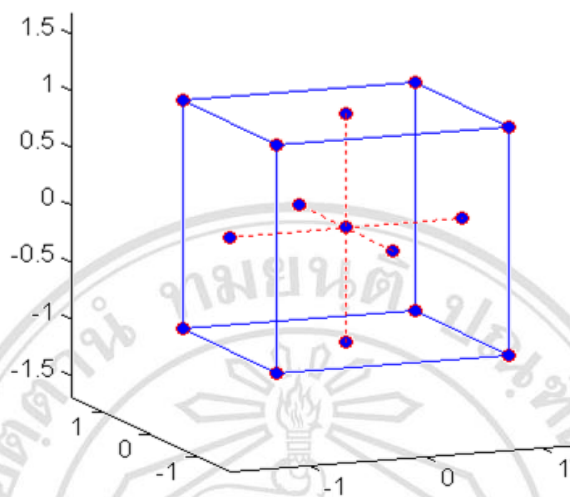


**Figure 1.6** The central composite face centered (CCF) design for three factors [30].

## 1.6 Multivariate Calibration

Multivariate calibration is a chemometric method designed for quantitative analysis [31]. It is an important analytical tool in many different fields of application such as food chemistry, pharmaceutical analysis, environment, agriculture and industrial. Many methods for multivariate calibration have been proposed such as multiple linear regression (MLR), principal component regression (PCR), response surface methodology (RSM) and locally weighted regression (LWR). The two multivariate methods that will be used in this research are multiple linear regression (MLR) and response surface methodology (RSM) [32-33].

### 1.6.1 Multiple Linear Regression (MLR)

In a simple linear regression, a single output parameter (Y) is related to a single input parameter (X) for each observation. In most problems, more than one input parameters are available. This problem leads to the multiple regression [34]. Multiple linear regression (MLR) is one of common techniques for calibration and regression both in chemistry and statistics. This method is carried out to predict the output



parameter (Y), given a set of p input parameters ( $X_1, X_2, X_3, \dots, X_p$ ). In multiple linear regression, p input parameters and the relationship between the output parameter and the input parameters is represented by the following equation:

$$Y = \beta_0 + \beta_1 X_1 + \beta_2 X_2 + \dots + \beta_p X_p + e \quad (1.9)$$

where:

$\beta_0$  is the constant term

$\beta_1$  to  $\beta_p$  are the coefficients relating the p independent variables to dependent variable (regression coefficient)

$e_i$  is the residual terms of the model and the distribution assumption (error or residual)

More complex models may include higher powers of independent variables or interaction effects of two or more variables. It can be written down to a model by the following form [28,31].

$$Y = \beta_0 + \beta_1 X + \beta_2 X^2 + e \quad (1.10)$$

or

$$Y = \beta_0 + \beta_1 X_1 + \beta_2 X_2 + \beta_{12} X_1 X_2 + e \quad (1.11)$$

### 1.6.2 Response surface methodology (RSM)

Response surface methodology (RSM) was developed by Box and his co-workers in the 50s. Response surface methodology consists of a group of mathematical and statistical techniques that based on the fit of empirical models to the experimental data obtained in relation to experimental design. The objective of RSM is to optimize a response which is influenced by several input parameters. Toward this objective, linear or square polynomial functions are employed to describe the system and, consequently, to explore experimental conditions through its optimization. Normally, the relationship between response and parameters is unknown, however it can be approximated by a low-degree polynomial model using the following form:

$$Y = f'(x) \beta + \varepsilon \quad (1.12)$$

where:

$f(x)$  is a vector function of  $p$  elements that consists of powers and cross-products of powers of  $x_1, x_2, \dots, x_k$  up to a certain degree denoted by  $d (\geq 1)$

$\beta$  is a vector of  $p$  unknown constant coefficients referred to as parameters

$\varepsilon$  is a random experimental error assumed to be a zero in average.

Two important models are commonly used in RSM. The simplest model are shown in equation 1.5.

$$Y = \beta_0 + \sum_{i=1}^K \beta_i x_i + \varepsilon \quad (1.13)$$

and the second-degree model ( $d = 2$ )

$$Y = \beta_0 + \sum_{i=1}^k \beta_i x_i + \sum \sum_{i < j} \beta_{ij} x_i x_j + \sum_{i=1}^k \beta_{ii} x_i^2 + \varepsilon \quad (1.14)$$

The surface represented by  $f(x_1, x_2)$  is called a response surface. The response can be indicated graphically, either in the three-dimensional or contour plots that assist in visualizing the shape of response surface. Contours are curve of constant response drawn in the  $x_i$  and  $x_j$  plane maintaining all outer parameters fixed [35-36]. Each contour corresponds to a particular height of the response surface, as indicated in Figure 1.7.

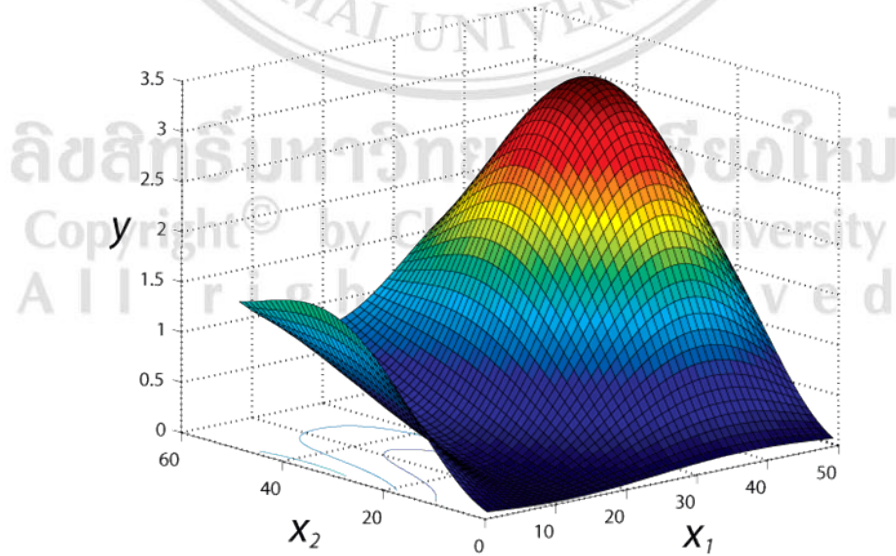


**Figure 1.7** Example response surface plot with two factors [37].

## 1.7 X-Ray Fluorescence Spectrometry (XRF)

X-ray fluorescence spectrometer is one of the most effective instruments usable by the analyst for the identification and measurement of major and trace elements in complex samples. However, this method cannot determine the elements lighter than sodium and only marginal below calcium. X-ray fluorescence method is nondestructive and can be used for the analysis of painting, archaeological specimens, jewelry, coins, and other valuable objects without harm to the sample. Moreover, this method is also widely applied for quality control in the manufacture of metals and alloys [38-39].

X-ray fluorescence analysis is based on the measurement of wavelengths and intensities of X-rays emitted by sample when excited by radiations from primary X-rays tube. Primary X-rays from tube provide sufficient energy to remove K, L or M electrons from the sample atoms. Subsequent movement of electrons from outer levels into these vacant positions gives rise to the emission of characteristic X-ray radiation of exact wavelengths [40]. The X-ray fluorescence process is shown in Figure 1.8.

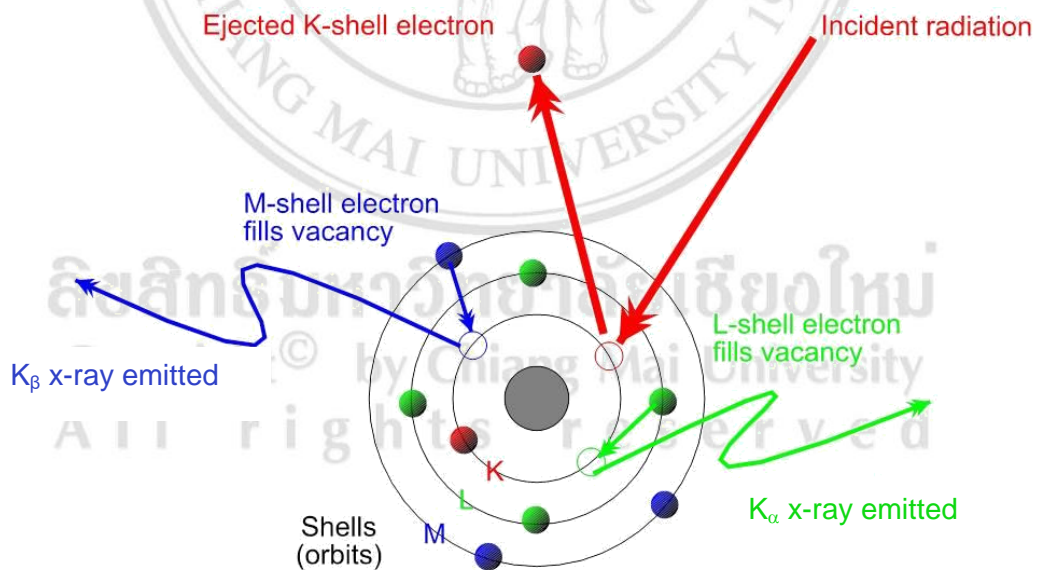


**Figure 1.8** The X-ray fluorescence process [41].

X-ray fluorescence instruments are often explained as wavelength dispersive instruments or energy dispersive instruments, depending on the method by which they resolve spectra [38].

Wavelength dispersive X-ray fluorescence provides the highest sensitivity and resolution. The wavelength dispersive X-ray fluorescence spectrometer schematic is shown in Figure 1.9. In this type of instrument, a primary X-ray beam irradiates the sample causing it to fluoresce. Each element emits its own characteristic X-rays. Part of the characteristic X-rays is collimated by a system of slits on to analyzing crystal. The crystal of known inter-planar spacing is mounted on a turntable which can be rotated by a motor. As the crystal rotates, the angle of crystal is changed in accordance with the Bragg's law. Part of beam is reflected by the crystal. The reflected beam passes through a set of collimating slits and enters the detector [40]. The reflective wavelength dispersive crystals which are used for X-ray analysis obey the Bragg equation:

$$n\lambda = 2d \sin\theta \quad (1.15)$$

where  $n$  is the order of reflection,  $\lambda$  is the wavelength of the incident X-ray,  $d$  is the interplanar spacing of the crystal and  $\theta$  is the angle of incidence [42].

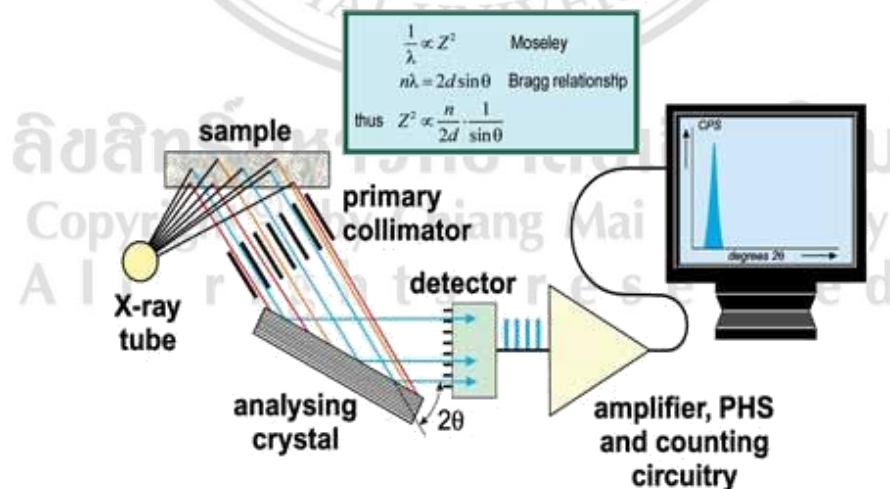


**Figure 1.9** The diagram of wavelength dispersive X-ray fluorescence spectrometer [43].

Energy dispersive X-ray fluorescence system is simplicity and lack of moving part in the excitation and detection components of the spectrometer. Energy dispersive instruments depend on the availability of detectors that respond to the energy of incident photons. This requirement must be carefully distinguished from respond to total incident energy or power, which is a function of both energy per photon and the number of photon received per unit time. The schematic of energy dispersive X-ray fluorescence spectrometer is shown in Figure 1.10. In this type of instrument, the X-rays characteristic from a sample irradiated with a primary X-ray beam enter a cooled Si(Li) detector which is connected to an amplifier system. It is necessary to cool the detector to liquid nitrogen temperatures in order to reduce electronic noise, and to ensure optimum resolution. The detector performs as a transducer converting x-ray photons to charge producing which is directly proportional to the energy of the X-ray that entering the detector [39-40].

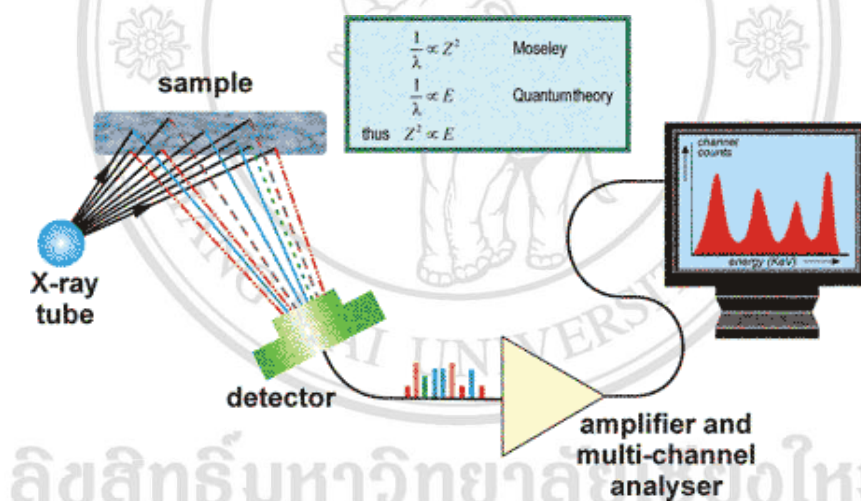


**Figure 1.10** The energy dispersive X-ray fluorescence spectrometer schematic [43].

The X-rays fluorescence spectrometry is very precise and accurate method. The method is attractive for elements that not reliable to wet chemistry method. However, the X-rays fluorescence method is difficult to detect an element present less than one part in 10,000 [42].



## 1.8 X-Ray Diffraction Spectrometry (XRD)

X-ray diffraction spectrometry is suitable for analyzing the crystalline materials [44]. This method is used to determine the spacing between atoms in crystalline sample. The interatomic spacings are used to infer crystalline structure. Furthermore, X-ray diffraction method can distinguish different crystalline forms of the same compound [42,45]. X-ray diffraction technique is based on constructive interference of monochromatic X-rays and a crystalline sample [46]. While the monochromatic X-rays were directing at the crystalline sample. The interaction of the monochromatic X-ray with sample produced constructive interference and diffractive rays. The incident angle at which X-rays are diffracted from crystalline sample is related to the atomic spacing in the crystal and the wavelength of the reflected rays. The X-ray diffraction process is shown in Figure 1.11. The condition for diffraction of a beam of X-ray from crystal is given by the Bragg equation [45].

$$n\lambda = 2d \sin\theta \quad (1.16)$$

When  $n$  is the order of diffraction,  $\lambda$  is the wavelength of X-ray beam,  $d$  is the interplanar of distance, and  $\theta$  is a different angle [47].

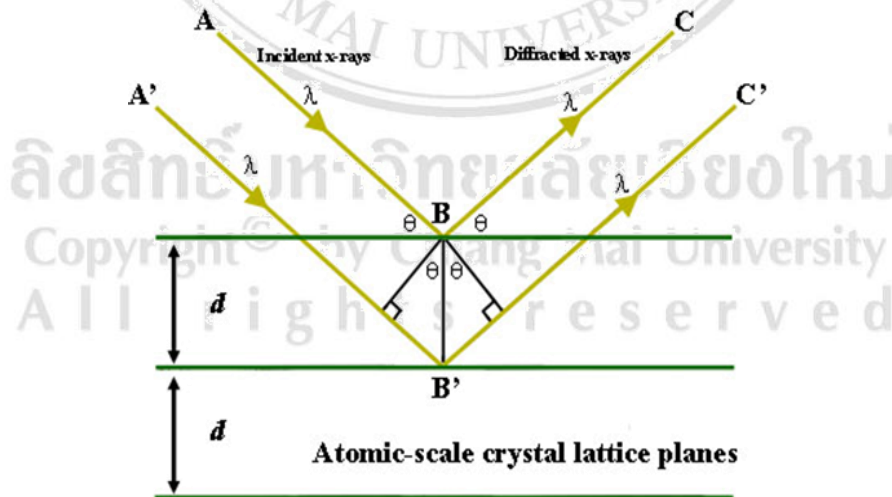


**Figure 1.11** The X-ray diffraction process [48].

The X-ray diffraction spectrometer diagram is shown in Figure 1.12. X-ray diffraction spectrometer consists of 3 basic compositions namely, X-ray tube, sample holder and X-ray detector. X-rays are generated in a cathode ray tube. X-rays from cathode ray tube are filtered by crystal monochromators to produce monochromatic X-rays needed for diffraction. These monochromatic X-rays are collimated and directed onto the sample. As the sample and detector are rotated, the intensity of diffracted X-ray is recorded. The X-ray diffraction patterns that are obtained by X-ray diffraction spectrometer can be used to identify the components of sample by comparison with Joint Committee on Powder Diffraction Standard (JCPDS) data base [44].

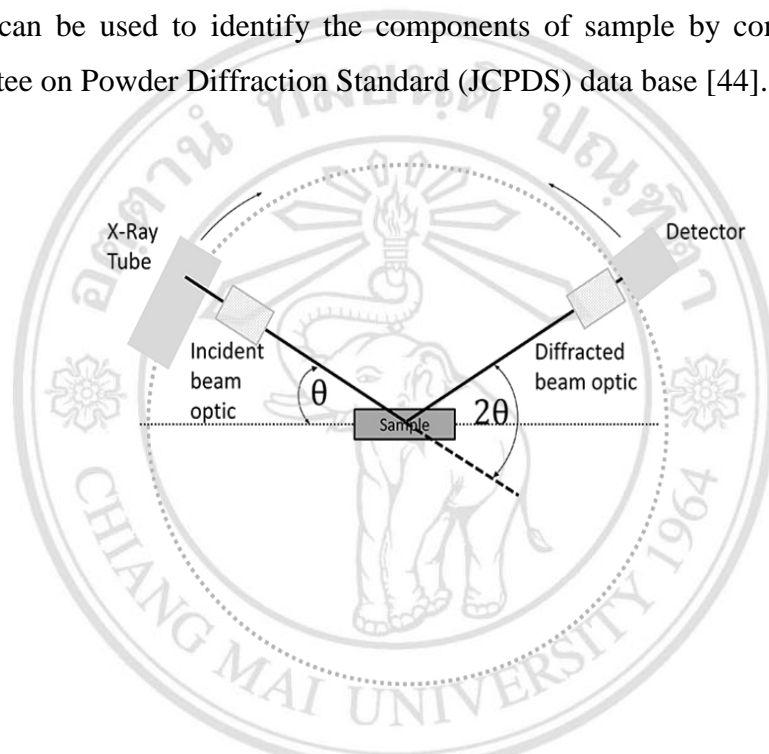


**Figure 1.12** The X-ray diffraction spectrometer diagram [49].

This method is nondestructive and only requires a small amount of sample. Furthermore, this technique is adaptable to quantitative applications because the intensities of the diffraction peaks of a given compound in a mixture are proportional to the fraction of the material in the mixture [31].

### 1.9 Fourier Transform Infrared Spectrometry (FT- IR)

Fourier transform-infrared spectrometry (FT-IR) is a preferred method of infrared spectroscopy [50]. Fourier transform infrared spectroscopy is based on the reaction between infrared radiation and absorbed molecules. The infrared radiation encompasses a section of the electromagnetic spectrum. The infrared region includes radiation at

wavenumbers between 14,000 to 20  $\text{cm}^{-1}$  or wavelengths between 0.4 to 500  $\mu\text{m}$ . Figure 1.13 shows the infrared region in the electromagnetic spectrum. The infrared region is usually divided into three sub-regions namely, near-infrared region (12,800-400  $\text{cm}^{-1}$ ), middle-infrared region (4000-200  $\text{cm}^{-1}$ ), and far-infrared region (200-10  $\text{cm}^{-1}$ ) [45,51].

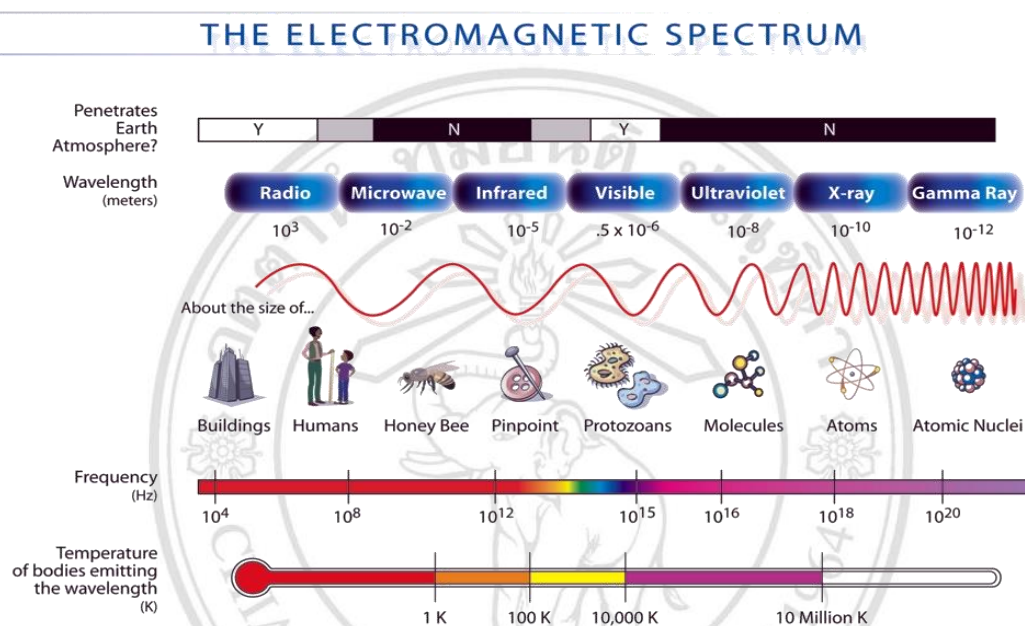


**Figure 1.13** The diagram of electromagnetic spectrum [52].

As molecules absorb infrared radiation, molecules are excited to a higher energy state. They absorb only selected frequencies of infrared radiation. The absorption of infrared radiation corresponds to energy changes in the order of 8 to 40 kJ/mole. Radiation of this energy range corresponds to the range encompassing the stretching and bending vibrational frequencies of the bonds in most covalent molecules [53].

The diagram of fourier transform-infrared spectrometer is shown in Figure 1.14. The fourier transform infrared spectrometer uses an interferometer to process the energy sent to the sample [53]. The interferometer consists of a beam splitter, moving mirror, and fixed mirror. Radiation from the infrared source is collimated by a mirror and the resultant beam is divided at the beam splitter [54]. Beam splitter is a mirror which is placed at a  $45^\circ$  angle to the incoming radiation. As the incoming radiation pass through



a beam splitter, half the beam passes to a fixed mirror and half is reflected to the moving mirror. The motion of the mirror causes the pathlength that the second beam traverse to vary. After reflection, the two beams recombine at the beam splitter. As two beams meet at the beam splitter, the pathlength differences of the two beams cause both constructive and destructive interferences. The combined beam containing these interference patterns is called the interferogram. An interferogram is the fundamental measurement obtained by fourier transform-infrared spectrometer. This interferogram contains all of the radiative energy coming from source and provides a wide range of wavelengths. The interferogram is oriented toward the sample by beam splitter. As interferogram passes through the sample, the sample simultaneously absorbs all of wavelengths that are found in its infrared spectrum. The modified interferogram signal that reaches the detector contains information about energy extent that was absorbed at every wavelength. The final interferogram contains all of the information in one time-domain signal, a signal that cannot be perceived by human. A mathematical process called a fourier transform implemented by computer to extract the individual frequencies that were absorbed and to reconstruct and plot infrared spectrum [45,53-55].

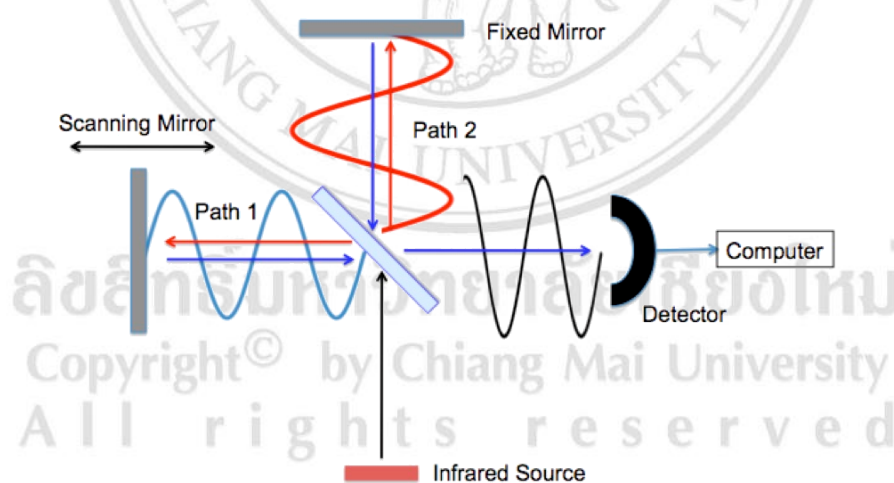


**Figure 1.14** The diagram of The Fourier Transform Infrared spectrometer [54].

Fourier transform infrared instrument contributes several significant advantages over dispersive instrument. Two of these are the Fellgett's advantage and Jacquinot's advantage. The Fellgett advantage is an improvement in signal to noise ratio per unit time, proportional to the square root of the number of resolution element being

observed. This results from the large number of resolution elements being observed simultaneously. In addition, Fourier transform infrared instrument dose has no slit, the total source output can be passed through the sample continuously. This results in a substantial gain in energy at the detector, therefore resulting in a higher signal to noise ratio. This is known as Jacquinot's advantage. Moreover, fourier transform spectrometers are faster than dispersive instrument. Therefore, these spectrometers are especially used in situations that require rapid and repetitive scanning. However, fourier transform spectrometers are still more expensive than dispersive instruments due to the precision needed for mirror movement and the computer that is also required [53].

#### **1.10 Scanning Electron Microscope (SEM) Equipped with Energy-Dispersive X- ray Spectroscopy (EDX)**

Scanning electron microscope is an essential surface characterization method. This method can be thought of as providing images of external morphology, similar to those accessed by the human eye [38]. The scanning electron microscope uses a focused beam of high-energy electrons to generate a variety of signals at the surface of solid samples. The signals that derive from electron-sample interactions reveal information about the sample including external morphology, chemical composition, crystalline structure and orientation of materials making up the sample [56]. The schematic of scanning electron microscope instrument is shown in Figure 1.15.

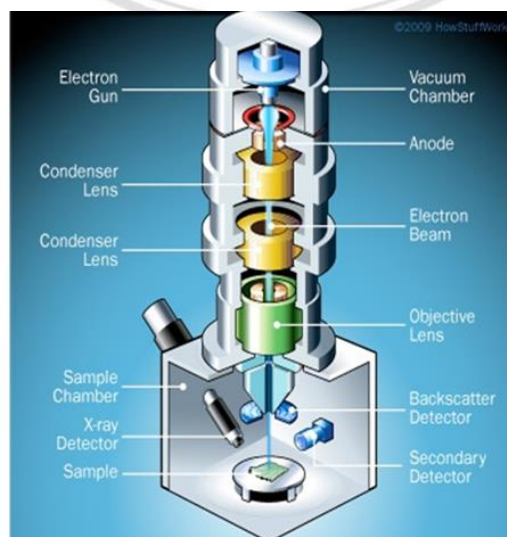


**Figure 1.15** The schematic of scanning electron microscope instrument [57].

Essential components of scanning electron microscope consist of electron gun, electron lenses, apertures, sample stage, electron beam, scanning coils, signal detectors for all signals of interest and data output devices. The basic principle is that the electrons from electron gun are accelerated to energy between 1-30 keV. The diameter of electron beam produced by electron gun is too large to form a high resolution image. Thus, the magnetic condenser and objective lens systems reduce the spot size to diameter of 2-10 nm when it reaches the sample. The condenser lens system is responsible for throughput of the electron beam reaching the objective lens. The objective lens determines the size of the beam hitting the sample surface. The beam of electrons is scanned across the sample in faster scan by scan coils [38,58]. A normal scanning electron microscope operates at a high vacuum because high vacuum environment allows electron travel without scattering by the air [51,58]. Image formation in the scanning electron microscope depends on the acquisition of signals produced from the electron beam and sample interactions. The interaction of the electron beam with a specimen occurs within an excitation volume under the specimen surface. The depth of the interaction volume depends on the composition of the solid specimen, the energy of the incident electron beam, and the incident angle [58]. Figure 1.16 shows the signal that can be used to obtain information in the surface topography. The three of these signals are important, namely secondary electron, backscattered electron and X-ray emission. The secondary electrons are most valuable for showing morphology and topography on sample. The backscattered electrons are most valuable for illustrating contrast in composition in multiphase samples and the characteristic X-rays that are used for elemental analysis [55].

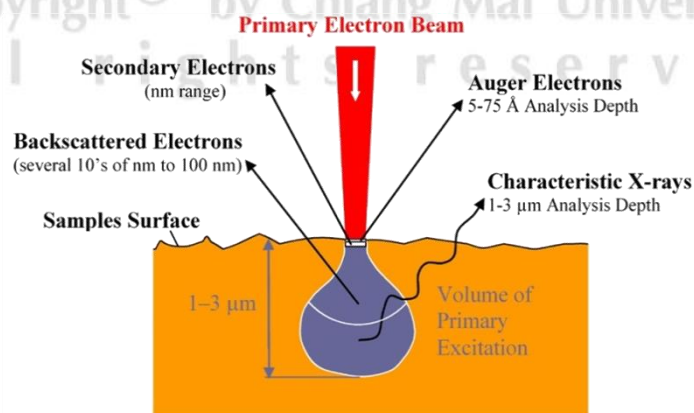


**Figure 1.16** Scanning electron microscopy scheme [59].

Energy dispersive X-ray spectroscopy (EDS or EDX) is a chemical microanalysis technique used in conjunction with scanning electron microscopy. This technique detects X-ray emitted from the solid sample during bombardment by high energy electron to characterize the elemental composition of the sample. All elements from atomic number 4 (Be) to 92 (U) can be detected in principle. Energy dispersive X-ray spectroscopy can be both a qualitative and quantitative measurement technique. In qualitative measurement, this technique involves the identification of line in the spectrum. In quantitative measurement, this technique measures line intensities for each element in the solid sample and for the same elements in calibration standards of known compositions. Energy dispersive X-ray spectroscopy system consists of X-ray detector, liquid nitrogen and software to analyze spectra. The most common detector is silicon lithium Si(Li) detector. Energy dispersive X-ray spectrum is described as plot of X-ray counts versus energy. Energy peaks correspond to the elements in sample. Thus, this spectrum can be used to determine the compositions of sample [60-62].

### **1.11 Gravimetric method**

Gravimetric analysis is one of the most accurate and precise methods of the macro-quantitative analysis. These methods are based on determining the mass of pure compound to which the analyte is chemically related. Gravimetric methods have been developed for most inorganic anions and cations, as well as for such a neutral species as water, sulfur dioxide, carbon dioxide, and iodine. A variety of organic substances can also be determined gravimetrically such as lactose in milk product, cholesterol in cereals, and salicylates in drug preparations. There are two major types of gravimetric method, namely precipitation methods and volatilization methods [63-64].

In precipitation gravimetry, the analyte is converted to a sparingly soluble precipitate. The precipitate is then filtered, washed free from impurities. The separated precipitate is dried or ignited and is accurately weight. From the weight of precipitate and a knowledge of its chemical composition, the weight of analyte in the desired from is calculated. However, the analyte is almost always weigh in different form. Therefore, calculation the weight of the desired substance from the weight of gravimetric precipitate can be done by using gravimetric factor [64].

$$\text{Gravimetric factor} = \frac{\text{formula weight of substance sought}}{\text{formula weight of substance weight}} \times \frac{a}{b} \quad (1.17)$$

Gravimetric factor is an appropriate ratio of formula weight of the substance sought to that of the substance weight, where a and b are integers that make the formula weight in the numerator and denominator chemically equivalent. The weight of substance sought is obtained by multiplying the weight of the precipitate by the gravimetric factor.

$$\text{sought (g)} = \text{weight (g)} \times \text{gravimetric factor} \quad (1.18)$$

Calculation is usually made on percentage. A general formula for calculating the percentage of the substance sought: [43].

$$\% \text{ sought} = \frac{\text{weight of precipitate (g)} \times \text{gravimetric factor}}{\text{weight of sample}} \times 100 \quad (1.19)$$

In volatilization gravimetry, the analyte or its decomposition products are volatilized at a suitable temperature. In the direct determination, the volatile product is collected on any of several solid desiccants and its mass is determined from the mass gain of the desiccant. An indirect method, the amount of volatile product is determined by measuring the loss in the mass of the sample during heating [64].

Gravimetric methods do not require a calibration or standardization step because the results are calculated directly from the experimental data and atomic mass. However, the gravimetric method takes time for each determination and cannot be automated. For these reasons, the gravimetric method is not often found on a routine basis [65-66].

### **1.12 Literature Review for Tungsten Extraction from Scheelite and Composite Scheelite**

Various methods have been proposed for extracting tungsten from scheelite ore. In classical process, acid decomposition with hydrochloric acid is usually employed to react with scheelite ore to produce colloidal solution of tungstic acid. In modern process, sodium carbonate or sodium hydroxide through an autoclaved process is used

to dissolve tungsten from scheelite ore. This method provides tungsten in form of sodium tungstate. This modern process is widely applied on commercial scale [2-3,67]. There are many publications which reported on the extraction tungsten from scheelite with alkalines [68-69]. In 2011, Zhongwei Zhao *et al.*[68] developed technology for extraction tungsten from scheelite concentrate by sodium hydroxide with autoclaved process. For this method, scheelite concentrate and sodium hydroxide were added to the autoclave for digestion. They found that the optimum conditions for digestion were 160 °C, digestion time was 2 hours, stirring speed was 400 rpm, sodium hydroxide dosage of 2.2 times and liquid/solid ratio of 0.8/1. They obtained sodium tungstate solution after 2 hours. Then, the solution was evaporated and changed to sodium tungstate crystalline that separated from contaminants in the main solution. This new technology can be applied to various kinds of tungsten ore such as scheelite middling and wolframite-scheelite mixed concentrate. In addition, the sodium hydroxide in main solution can be reused for leaching again.

In 2011, Zhongwei Zhao *et al.*[69] studied using the twin screw extruder for digestion scheelite with sodium hydroxide. In this method, scheelite concentrate was added to a certain quantity of sodium hydroxide to obtained mixture slurry. Then, the mixture slurry was mixed by twin screw. They found that the optimum conditions for leaching were 120 °C, leaching time was 3.5 hours, screw rotating speed was 160 rpm and sodium hydroxide dosage of 2.2 times. Tungsten in scheelite ore changed to sodium tungstate solution. Using the screw helped mass transfer and reduced temperature for leaching as compared to the conventional sodium hydroxide leaching.

In addition, there are many publications reported on the extraction tungsten from composite scheelite with alkalines [70-72]. In 2000, K. Srinivas *et al.*[70] studied extraction of tungsten from multi-metal tin-tungsten ore by physical benefit with sodium hydroxide roast-liquors leach process. In this method, tin was separated by physical benefit process. Next, tungsten was extracted from composite wolframite-scheelite concentrate. The extraction process divided into roasting and leaching. In roasting process, composition wolframite-scheelite concentrate was roasted in furnace with sodium carbonate and sodium nitrate. They found that the optimum conditions for roasting were 550 K, roasting time was 2 hours and sodium carbonate/feed mass ratio of 1/1.5. The roasted mass was obtained. The leaching process exhibits 2 steps. In the first

step, the roasted mass was leached by hot water 100 ml to produce leaching solution and residue. In the second step, the residue was leached by hot water 50 ml. They found that optimum conditions for both two leaching steps were 343 K, leaching time was 30 minutes, pH 12 and 343 K, leaching time was 30 minutes, pH 10.5, respectively. Finally, tungsten in leach liquors and residues were analyzed by spectrophotometer.

In 2004, Li Hong Gui[71] developed the novel process for tungsten recovery from high molybdenum scheelite concentrate by sodium hydroxide digestion with selective precipitation process. In this process, scheelite was digested by sodium hydroxide to obtain sodium tungstate solution. Next, ammonium chloride was added to the sodium tungstate solution to produce ammonium paratungstate solution with molybdenum, tin and arsenic contamination. Then, the complex sulfide of nonferrous metals as selective precipitation was added to the impure ammonium paratungstate solution for precipitated impurities from solution. Finally, pure ammonium paratungstate solution was evaporated to obtain ammonium paratungstate crystalline. The novel process can produce 95% ammonium paratungstate crystalline. This process was confirmed by Chinese National Standard GB100116-88APT. In addition, this novel process has been applied in many industrial plants in China.

In 2016, Yalei Wang *et al.*[72] studied leaching tungsten from composite barite-scheelite concentrate. In this method, scheelite concentrate was added in crucible with sodium carbonate and silicon dioxide. Next, sample in crucible was roasted in electric box furnace. They found that the optimum conditions for roasting were 850 °C, roasting time was 2 hours, silicon dioxide/feed mass ratio of 10% and sodium carbonate/tungsten molar ratio of 1/3. They obtained the solution containing tungsten after 2 hours. Then, the solution was leached by sodium carbonate. They found that the optimum conditions for leaching were 60 °C, leaching time was 2 hours, stirring speed was 300 rpm, liquid/solid ratio of 5/1 and sodium carbonate/solution of 10 g/L. These leaching solution and residue were analyzed by Inductively Coupled Plasma-Atomic Emission Spectroscopy (ICP-AES) for determination of tungsten. The residue was analyzed by X-ray diffraction for components investigation. This method can be applied to low-grade scheelite, wolframite and composite ore. In these researches, the extraction of tungsten from scheelite and composite scheelite using alkaline exhibits complex procedure, required high leaching temperature and required large amount of reagent.



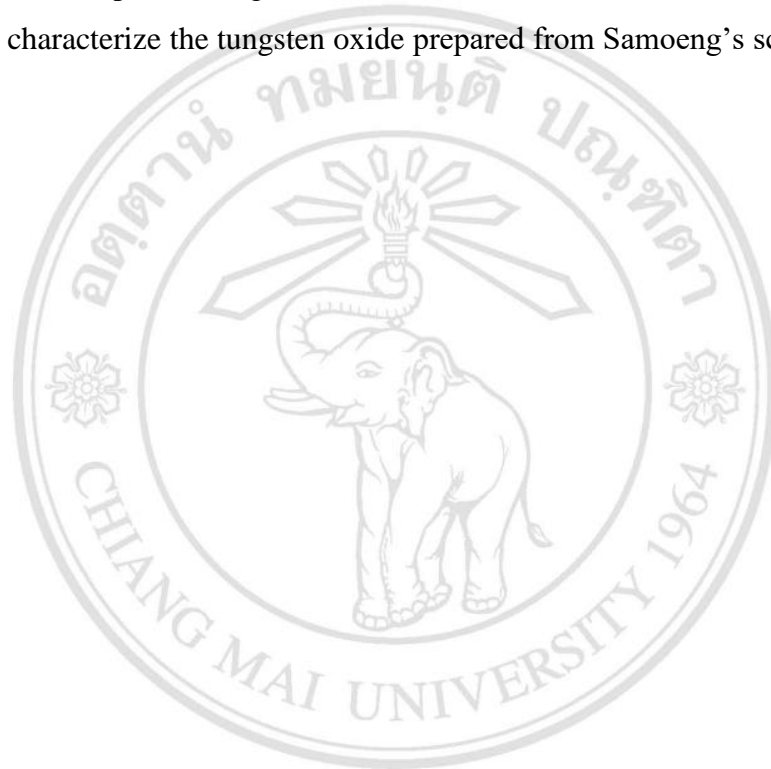
There are many researches which reported on the extraction of tungsten with acid and chelating agent [5,73]. In 1999, Sebahattin Gurmen *et al.*[73] studied using the chelating agent to leach low grade scheelite concentrate with hydrochloric acid. From this method, scheelite concentrate was leached by hydrochloric acid with phosphoric acid as chelating agent. As a result, tungsten in scheelite sample was dissolved in acid solution. They found that the optimum conditions for leaching were 80 °C, leaching time was 2 hours, stirring speed was 900 rpm, the weight ratio between W and  $\text{PO}_4^{3-}$  was 7 to 1, solid/liquid ratio of 1/10 and concentration of hydrochloric acid used was 2 M. The leaching solution was analyzed by atomic absorption spectroscopy (AAS) for determination of tungsten. Then, the solution was precipitated by ammonium hydroxide to produce triammonium-dodeca tungstato-phosphate salt. This method had fewer steps as compared to the conventional acid method because it didn't need to evaporate in the APT process. However, hydrochloric acid is highly corrosive. It can corrode equipment.

In 2015, Wenjuan Zhang *et al.*[5] studied kinetic of the dissolution of scheelite and the effects of parameters on leaching tungsten from scheelite concentrate. In this method, tungsten in scheelite concentrate was dissolved by nitric acid with phosphoric acid acting as chelating agent to produce phosphotungstic acid. This solution was analyzed by Inductively Coupled Plasma-Optical Emission Spectrometer (ICP-OES). They found that the optimum conditions for leaching were 363 K, leaching time was 2 hours, 3 M nitric acid concentration, 0.1 M phosphoric acid concentration and particle size of scheelite concentrate was 35-50  $\mu\text{m}$ . Next, microporous weak-base anion exchange resin D301 was added to phosphotungstic acid solution to produce ammonium tungstate solution. Then, magnesium chloride was added to ammonium tungstate solution for separation of phosphorus. Finally, the solution was evaporated to obtain ammonium paratungstate crystalline. The extraction with nitric acid provides various advantages such as less corrosive when compare with that of hydrochloric acid and wastewater from this process can be treated as nitrogen fertilizer.



### 1.13 Research Objectives

1. To study and develop process for tungsten oxide preparation from Samoeng's scheelite ore.
2. To investigate the effects of parameter, namely  $\text{HNO}_3$  concentration, leaching temperature, leaching time,  $\text{W}/\text{PO}_4^{3-}$  weight ratio, calcination temperature and calcination time on the recovery of tungsten oxide using central composite design (CCD).
3. To characterize the tungsten oxide prepared from Samoeng's scheelite



ลิขสิทธิ์มหาวิทยาลัยเชียงใหม่  
Copyright© by Chiang Mai University  
All rights reserved

## LIST OF ABBREVIATION AND SYMBOLS

g	gram
°C	degree Celsius
m <sup>3</sup>	cubic meter
cm <sup>3</sup>	cubic centimeter
JCPDS	Joint Committee on Powder Diffraction Standard
cm <sup>-1</sup>	inverse centimeter
kJ	kilojoules
rpm	revolution per minute
K	kelvin
ml	milliliter
M	molar (mol per liter)
APT	ammonium paratungstate
μm	micrometer
wt%	weight percent
XRF	X-Ray Fluorescence Spectroscopy
WDXRF	Wavelength Dispersive X-ray Fluorescence Spectroscopy
XRD	X-Ray Diffraction Spectroscopy
FTIR	Fourier Transform Infrared Spectroscopy
SEM	Scanning Electron Microscopy
EDX	Energy Dispersive X-ray Spectroscopy
Å	angstrom
nm	nanometer

## CHAPTER 2

### Experimental

#### 2.1 Apparatus and Chemicals

##### 2.1.1 Material

Scheelite ore sample was provided by Department of Primary Industries and Mines, Chiang Mai Province, Thailand. The phase compositions of scheelite concentrate sample were analyzed by X-ray diffraction spectrometer. X-ray diffraction pattern of scheelite concentrate sample is shown in Figure 2.1. As seen in Figure 2.1, X-ray diffraction pattern of scheelite concentrate sample matches with standard X-ray diffraction pattern of scheelite ( $\text{CaWO}_4$ ) by JCPDS number 41-1431. The chemical compositions of scheelite concentrate sample were analyzed by X-ray fluorescence spectrometer. The main chemical compositions of scheelite concentrate for this experiment is presented in Table 2.1.

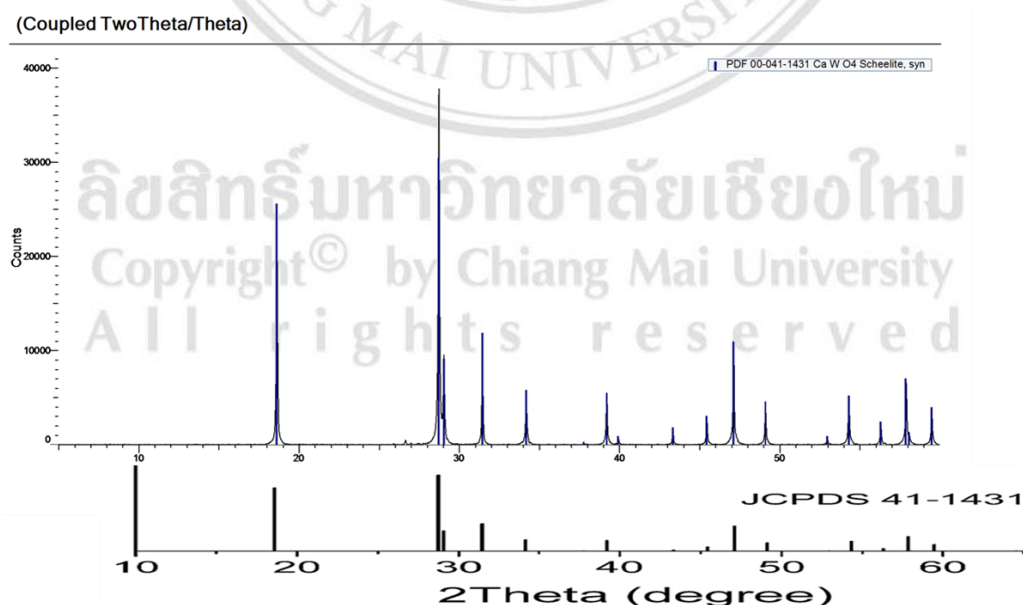


**Figure 2.1** The X-ray diffraction pattern of scheelite concentrate sample and standard X-ray diffraction pattern of scheelite.

**Table 2.1** The main chemical compositions of scheelite concentrate

Chemical composition	Content (Weight %)
WO <sub>3</sub>	77.0
CaO	17.6
SnO <sub>2</sub>	2.94
SiO <sub>2</sub>	0.895
Al <sub>2</sub> O <sub>3</sub>	0.324
ZrO <sub>2</sub>	0.232
SO <sub>3</sub>	0.149
P <sub>2</sub> O <sub>5</sub>	0.148
PbO	0.141
Fe <sub>2</sub> O <sub>3</sub>	0.104

**2.1.2 Apparatus**

- 1) Aluminum Hot Plate Stirrer, AREX Digital (VELP Scientifica, Italy)
- 2) Economic magnetic stirrer with stainless steel heating plate, Model RH basic 1(IKA, Germany)
- 3) Hot plate & Magnetic stirrer, model HY-HS11(HYSC, South Korea)
- 4) Thermometer
- 5) Magnetic bar
- 6) Filter paper, CAT No. 1001-125 (Whatman, United Kingdom)
- 7) Thermolyne™ Benchtop 1100°C Muffle Furnaces, Type 1400 (Thermo Fisher Scientific, United States of America)
- 8) D2 PHASER desktop diffractometer (Bruker, Germany)
- 9) JEOL JSM-6335F Field Emission Scanning Electron Microscope (JEOL, United States of America)
- 10) TENSOR 27 FT-IR spectrometer (Bruker, Germany)
- 11) Benchtop WDXRF Supermini 200 (Rigaku, United States of America)

### 2.1.3 Chemicals

- 1) Nitric acid, 65% (AR grade, RCI Labscan, Thailand)
- 2) Phosphoric acid 85% (AR grade)
- 3) Ammonia Solution, 28-30% (AR grade, Lobachemie, India)

## 2.2 Method

### 2.2.1 Scheelite Ore Beneficiation

Scheelite sample was obtained from Bo Keao mine in the form of ore. Ore from mine was treated for separating scheelite concentrate from waste rock and other mineral. The flow process chart of scheelite ore beneficiation shows in Figure 2.2. Firstly, ore from mine was crushed and milled. Then, ore powder was separated based on particle size using vibration screen and was separated based on weight using shaking table to obtain concentrates. Finally, scheelite concentrate was separated by high tension separator and frantz isodynamic magnetic separator for producing scheelite concentrate.

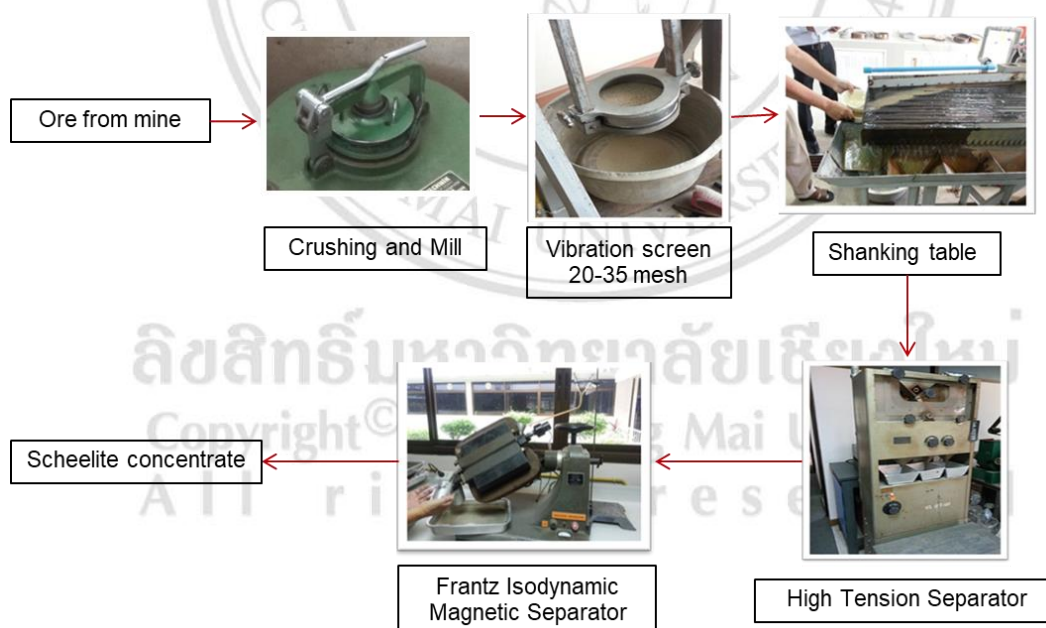


**Figure 2.2** Scheelite ore beneficiation process flow diagram.

### 2.2.2 Preparation of Tungsten Oxide

There are five process steps for tungsten oxide preparation from scheelite concentrate. The flowchart of preparation of tungsten oxide is shown in Figure 2.3. First, scheelite concentrate sample was weighed out about 2 grams and recorded the exact weight. Second, scheelite concentrates sample, nitric acid and phosphoric acid were placed into beaker and heated with stirs by thermostat for 120 minutes to produce phosphotungstic acid solution. Third, the phosphotungstic acid solution was filtered for separating the solid waste from solution. Fourth, ammonium hydroxide solution was added into filtrated solution for precipitating the tungstate salt. Finally, tungstate salt was calcined in the furnace at 600 °C for 30 minutes to produce tungsten oxide.



**Figure 2.3** Flowchart of tungsten oxide preparation.

### 2.2.3 Design of Experiments for Leaching Tungsten from Scheelite Concentrates

Various parameters were investigated in this research including concentrations of nitric acid, leaching temperature,  $W/PO_4^{3-}$  weight ratio, leaching time, calcination temperature and calcination time. However, the experiment was designed by 5 levels

circumscribed central composite design (CCD) for investigating effect of concentration of nitric acid, leaching temperature and  $W/PO_4^{3-}$  weight ratio on the recovery of tungsten oxide. The coded levels and actual levels of input parameters listed in Table 2.2.

**Table 2.2** Coded and actual levels of input parameters from central composite design

Experiment	Concentration of nitric acid ( $X_1$ )		Leaching temperature ( $X_2$ )		$W/PO_4^{3-}$ weight ratio ( $X_3$ )	
	Coded level	Actual level (M)	Coded level	Actual level ( $^{\circ}C$ )	Coded level	Actual level (mol/mol)
A	-1.000	2	-1.000	60	-1.000	4:1
B	-1.000	2	-1.000	60	1.000	12:1
C	-1.000	2	1.000	100	-1.000	4:1
D	-1.000	2	1.000	100	1.000	12:1
E	1.000	6	-1.000	60	-1.000	4:1
F	1.000	6	-1.000	60	1.000	12:1
G	1.000	6	1.000	100	-1.000	4:1
H	1.000	6	1.000	100	1.000	12:1
I	-1.682	0.64	0	80	0	8:1
J	1.682	7.36	0	80	0	8:1
K	0	4	-1.682	46.4	0	8:1
L	0	4	1.682	113.6	0	8:1
M	0	4	0	80	-1.682	1.28:1
N	0	4	0	80	1.682	14.72:1
O	0	4	0	80	0	8:1
P	0	4	0	80	0	8:1
Q	0	4	0	80	0	8:1
R	0	4	0	80	0	8:1

NOTE: The values in this table were calculated by central composite design.

Table 2.2 indicates that the concentration of  $HNO_3$ , leaching temperature and  $W/PO_4^{3-}$  weight ratio are varied in the ranges of 0.64-7.36 M, 46.4-113.6  $^{\circ}C$  and 1.28:1-14.72:1 mol/mol, respectively. The other parameters are fixed constants, namely leaching time for 120 minutes, calcination time for 30 minutes and calcination temperature of 600  $^{\circ}C$ .

#### **2.2.4 Optimization of Leaching Time**

First, scheelite concentrate sample was weighed out about 2 grams and recorded the exact weight. Second, scheelite concentrates sample, nitric acid and phosphoric acid were placed into beaker and heated with stirrer by thermostat for producing phosphotungstic acid solution. Leaching times at 90, 120 and 150 minutes were varied. Third, the phosphotungstic acid solution was filtered for separating the solid waste from solution. Fourth, ammonium hydroxide solution was added into filtrated solution for precipitating the tungstate salt. Finally, tungstate salt was calcined by furnace at 600 °C for 30 minutes to produce tungsten oxide.

#### **2.2.5 Optimization of Calcination Temperature**

First, scheelite concentrate sample was weighed out about 2 grams and recorded the exact weight. Second, scheelite concentrates sample, nitric acid and phosphoric acid were placed into beaker and heated with stirrer by thermostat for 120 minutes to produce phosphotungstic acid solution. Third, the phosphotungstic acid solution was filtered for separating the solid waste from solution. Fourth, ammonium hydroxide solution was added into filtrated solution for precipitating the tungstate salt. Finally, tungstate salt was calcined by furnace for 30 minutes to produce tungsten oxide. Calcination temperatures at 500, 600, 700 and 800 °C were varied.

#### **2.2.6 Optimization of Calcination Time**

First, scheelite concentrate sample was weighed out about 2 grams and recorded the exact weight. Second, scheelite concentrates sample, nitric acid and phosphoric acid were placed into beaker and heated with stirrer by thermostat for 120 minutes to produce phosphotungstic acid solution. Third, the phosphotungstic acid solution was filtered for separating the solid waste from solution. Fourth, ammonium hydroxide solution was added into filtrated solution for precipitating the tungstate salt. Finally, tungstate salt was calcined by furnace at 600 °C to produce tungsten oxide. Calcination times at 30, 45, 60 and 75 minutes were varied.



## **2.2.7 Characterization Techniques**

### **1) X-ray Fluorescence Spectroscopy (XRF)**

The compositions of Samoeng's scheelite concentrates were analyzed by X-ray fluorescence (XRF) method. XRF spectra were obtained by Benchtop WDXRF Supermini 200 (Rigaku, United States of America).

### **2) X-ray diffraction Spectroscopy (XRD)**

The phase transformation and crystallite size of the products were characterized by X-ray diffraction (XRD) method. X-ray diffraction pattern obtained using a D2 PHASER desktop diffractometer (Bruker, Germany).

### **3) Fourier Transform Infrared Spectroscopy (FTIR)**

Phase transformation was confirmed with Fourier Transform Infrared Spectroscopy (FTIR) method. The FTIR spectrum were obtained by TENSOR 27 FT-IR spectrometer (Bruker, Germany).

### **4) Scanning Electron Microscopy (SEM) equipped with Energy-Dispersive X-ray Spectroscopy (EDX)**

Morphology and compositions of products were characterized by Scanning Electron Microscopy (SEM) equipped with Energy-Dispersive X-ray Spectroscopy (EDX) method. The SEM images and compositions of products were obtained by JEOL JSM-6335F Field Emission Scanning Electron Microscope (JEOL, United States of America) using an electron beam energy of 15 keV.

Copyright© by Chiang Mai University  
All rights reserved

## CHAPTER 3

### Results and Discussion

#### 3.1 Central Composite Design

Based on central composite design, the effects of three parameters including, concentration of nitric acid, leaching temperature and  $W/PO_4^{3-}$  weight ratio on weight, color and percent recovery of tungsten oxide are shown in Table 3.1. The percent recovery of tungsten oxide, average percent recovery and standard deviations of all conditions are shown in Table 3.2.



ลิขสิทธิ์มหาวิทยาลัยเชียงใหม่  
Copyright© by Chiang Mai University  
All rights reserved

**Table 3.1** The effects of leaching conditions on weight, color and percent recovery tungsten oxide

Experiments	Concentration of nitric acid (M)	Leaching temperature (°C)	W/PO <sub>4</sub> <sup>3-</sup> weight ratio (mol/mol)	Replications	Sample weight (g)	Tungsten oxide weight (g)	Color	% recovery
A	2	60	4:1	1	2.1361	0.2460	White	15.0
				2	2.0256	0.1818	White	11.7
				3	2.0037	0.4706	Light green	30.5
B	2	60	12:1	1	2.0076	0.3564	Light yellow	23.1
				2	2.0253	0.5570	Light yellow	35.7
				3	2.0129	0.3856	Light yellow	24.9
C	2	100	4:1	1	2.0761	1.1985	Light yellow	75.0
				2	2.0229	1.7224	Light yellow	110.6
				3	2.0178	1.4258	Light yellow	91.8
D	2	100	12:1	1	2.0427	0.5293	Light blue	33.7
				2	2.083	0.7916	Light blue	49.4
				3	2.0057	0.7646	Light blue	49.5
E	6	60	4:1	1	2.0596	0.3509	Yellow	22.1
				2	2.0618	0.2467	Yellow	15.5
				3	2.0251	0.2626	Light blue	16.8

**Table 3.1** (continued)

Experiments	Concentration of nitric acid (M)	Leaching temperature (°C)	W/PO <sub>4</sub> <sup>3-</sup> weight ratio (mol/mol)	Replications	Sample weight (g)	Tungsten oxide weight (g)	Color	% recovery
F	6	60	12:1	1	2.0270	0.1843	Yellow	11.8
				2	2.0108	0.2659	Yellow	17.2
				3	2.0226	0.1975	Yellow	12.7
G	6	100	4:1	1	2.0579	0.5294	Yellow	33.4
				2	2.0987	0.5578	Yellow	34.5
				3	2.0358	0.4639	Yellow	29.6
H	6	100	12:1	1	2.0046	0.2781	Light brown	18.0
				2	2.0588	0.3345	Light blue	21.1
				3	2.0103	0.3567	Light brown	23.0
I	0.64	80	8:1	1	2.0204	0.5113	Light green	32.9
				2	2.0253	0.1808	White	11.6
				3	2.1066	0.5330	Light green	32.9
J	7.36	80	8:1	1	2.0338	0.1262	White	8.1
				2	2.0385	0.1362	Light yellow	8.7
				3	2.0125	0.1944	White	12.5

**Table 3.1** (continued)

Experiments	Concentration of nitric acid (M)	Leaching temperature (°C)	W/PO <sub>4</sub> <sup>3-</sup> weight ratio (mol/mol)	Replications	Sample weight (g)	Tungsten oxide weight (g)	Color	% recovery
K	4	46.4	8:1	1	2.0918	0.2232	Yellow	13.9
				2	2.0143	0.1867	Yellow	12.0
				3	2.0924	0.3059	Yellow	19.0
L	4	113.6	8:1	1	2.0345	0.4298	Blue	27.4
				2	2.0444	0.7062	Light blue	44.9
				3	2.0542	0.8626	White	54.5
M	4	80	1.28:1	1	2.0044	1.2636	Light green	81.9
				2	2.0808	1.6051	Light green	100.2
				3	2.014	1.7123	Light green	110.4
N	4	80	14.72:1	1	2.0263	0.4295	Light brown	27.5
				2	2.0871	0.4506	Light brown	28.0
				3	2.0368	0.4137	Light brown	26.4
O	4	80	8:1	1	2.0346	0.7450	Light yellow	47.6
				2	2.0238	0.9427	Light yellow	60.5
				3	2.0075	1.0034	Light yellow	64.9

**Table 3.1** (continued)

Experiments	Concentration of nitric acid (M)	Leaching temperature (°C)	W/PO <sub>4</sub> <sup>3-</sup> weight ratio (mol/mol)	Replications	Sample weight (g)	Tungsten oxide weight (g)	Color	% recovery
P	4	80	8:1	1	2.0332	0.8141	Yellow	52.0
				2	2.0114	0.5559	Yellow	35.9
				3	2.0128	0.9168	Light green	59.2
Q	4	80	8:1	1	2.0201	0.8898	Yellow	57.2
				2	2.0358	1.1995	Yellow	76.5
				3	2.0203	1.0957	Yellow	70.4
R	4	80	8:1	1	2.0620	1.0068	White	63.4
				2	2.0243	0.9857	Light yellow	69.2
				3	2.0545	0.9836	White	62.2

**Table 3.2** Percent recovery of tungsten oxide, means and standard deviations

Experiments	% Recovery			Average % Recovery
	1	2	3	
A	15.0	11.7	30.5	19.0 ± 10.1
B	23.1	35.7	24.9	27.9 ± 6.8
C	74.9	110.6	91.8	92.4 ± 17.8
D	33.7	49.4	49.5	44.2 ± 9.1
E	22.1	15.5	16.8	18.2 ± 3.5
F	11.8	17.2	12.7	13.9 ± 2.9
G	33.4	34.5	29.6	32.5 ± 2.6
H	18.0	21.1	23.0	20.7 ± 2.5
I	32.9	11.6	32.9	25.8 ± 12.3
J	8.1	8.7	12.5	9.8 ± 2.4
K	13.9	12.0	19.0	15.0 ± 3.6
L	27.4	44.9	54.9	42.4 ± 13.9
M	81.9	100.2	110.4	97.5 ± 14.5
N	27.5	28.0	26.4	27.3 ± 0.9
O	47.6	60.5	64.9	57.7 ± 9.0
P	52.0	35.9	59.2	49.0 ± 11.9
Q	57.2	76.5	70.4	68.1 ± 9.9
R	63.4	69.2	62.2	64.9 ± 3.8

Based on central composite design, the effects of three parameters including, concentration of nitric acid ( $X_1$ ), leaching temperature ( $X_2$ ) and  $W/PO_4^{3-}$  weight ratio ( $X_3$ ) on percent recovery of tungsten oxide ( $Y$ ) are studied by multiple linear regression (MLR). Multiple linear regression is used to calculate the correlation coefficient from experimental results. The correlation coefficients, which obtained from calculation, can show the relationship of concentration of nitric acid ( $X_1$ ), leaching temperature ( $X_2$ ) and  $W/PO_4^{3-}$  weight ratio ( $X_3$ ) on percent recovery of tungsten oxide ( $Y$ ). The correlation coefficients, which included quadratic coefficients, linear coefficients and interaction

coefficients, are illustrated in form of quadratic equation. The quadratic equation is given by the equation 3.1.

$$Y = -13.82X_1^2 - 10.13X_2^2 + 1.25X_3^2 - 8.19X_1X_2 + 2.83X_1X_3 - 7.65X_2X_3 - 8.79X_1 + 10.92X_2 - 12.14X_3 + 55.34 \quad (3.1)$$

This equation shows the significance of concentration of nitric acid ( $X_1$ ), leaching temperature ( $X_2$ ) and  $W/PO_4^{3-}$  weight ratio ( $X_3$ ) on percent recovery of tungsten oxide (Y) and viability of the developed model for prediction. In order to visualize the effects of parameters on the recovery of tungsten oxide, the parameters in equation 3.1 were replaced with their values within experimental ranges for creating response surface plots. This method is called Response Surface Methodology (RSM). Response surface plots were plotted by maintaining one parameter at its central level (coded level = 0), while varying two parameters for understanding their interactive and individual effect on percent recovery of tungsten oxide. A curvature in response surface plot showed that the response was sensitive to varying parameter, while aligned line showed that the response was insensitive to varying parameter. The effect of three parameters namely, concentrations of nitric acid ( $X_1$ ), leaching temperatures ( $X_2$ ) and  $W/PO_4^{3-}$  weight ratio ( $X_3$ ) on percent recovery of product (Y) were indicated in three dimensional view as shown in Figure 3.1.

ลิขสิทธิ์มหาวิทยาลัยเชียงใหม่  
Copyright© by Chiang Mai University  
All rights reserved



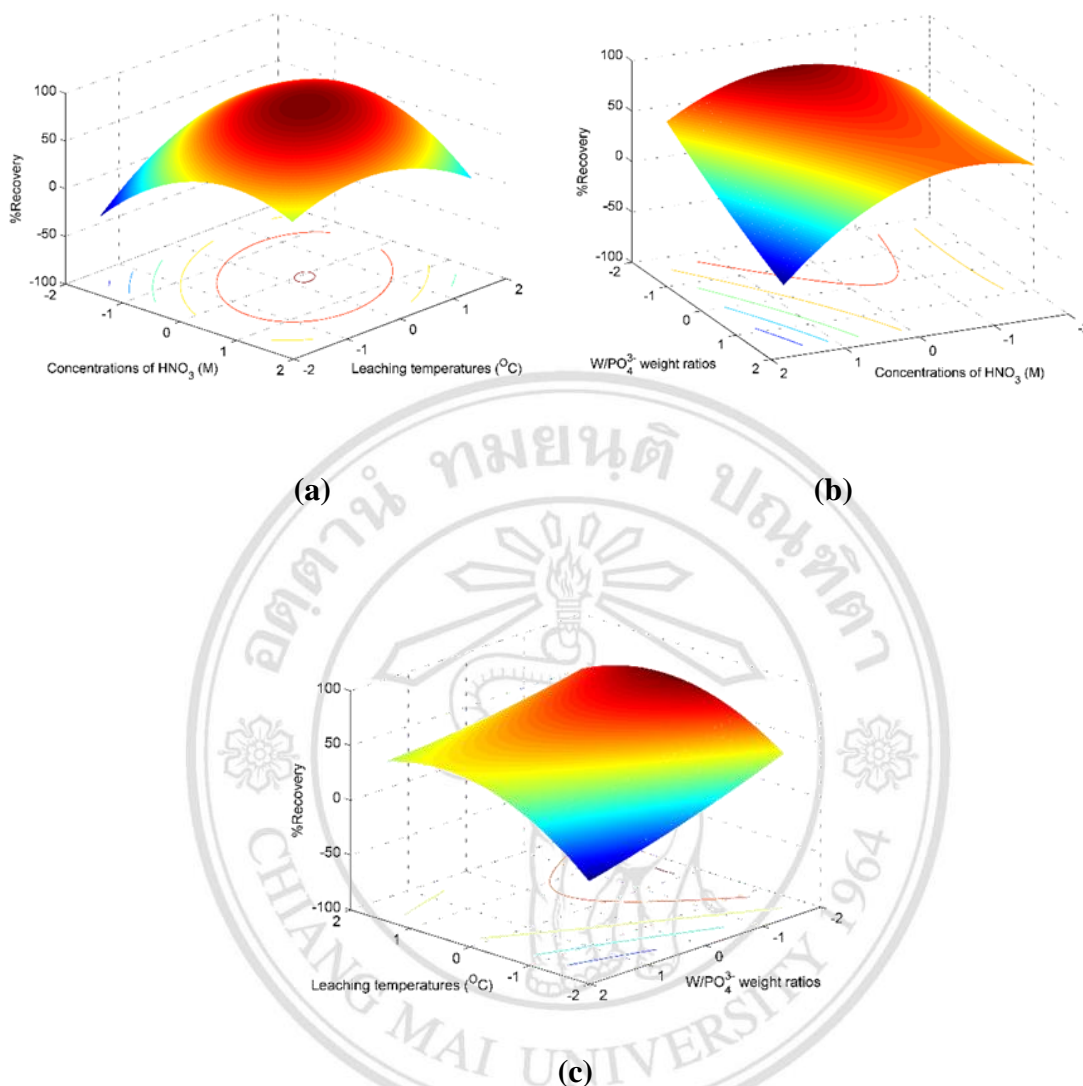


**Figure 3.1** Response surface plots: (a) Effect of concentration of nitric acid and leaching temperature on percent recovery of product; (b) Effect of concentration of nitric acid and W/PO<sub>4</sub><sup>3-</sup> weight ratio on percent recovery of product; (c) Effect of leaching temperature and W/PO<sub>4</sub><sup>3-</sup> weight ratio on percent recovery of product.

As presented in Figure 3.1, the optimum values of three parameters and maximum predicted values of response obtain from the red zone in response surface plots. As seen in Figure 3.1(a), the optimum of concentration of nitric acid and leaching temperature are near the central level. Figure 3.1 (b) showed the effects of W/PO<sub>4</sub><sup>3-</sup> weight ratio and concentration of nitric acid. At high concentration of nitric acid, W/PO<sub>4</sub><sup>3-</sup> weight ratio exhibited significant effect on the percent recovery of tungsten oxide because the percent recovery of tungsten oxide increased while the W/PO<sub>4</sub><sup>3-</sup> weight ratio decreased.

In this research, phosphoric acid is a chelating agent. The  $\text{PO}_4^{3-}$  anion would replace all four  $\text{O}^{2-}$  ions in scheelite concentrate ( $\text{CaWO}_4$ ) and lead to produce the water-soluble phosphotungstic acid ( $\text{H}_3\text{PW}_{12}\text{O}_{40}$ ). Thus, the increasing of solubility of tungsten causes the increasing of recovery of tungsten oxide. However, at low concentration of nitric acid, effect of  $\text{W}/\text{PO}_4^{3-}$  weight ratio is not significant. As shown in Figure 3.1 (c), the decreasing of  $\text{W}/\text{PO}_4^{3-}$  weight ratio exhibits a positive effect on the recovery of tungsten oxide. However, the recovery of tungsten oxide slightly decreases when the leaching temperature continually increase. The optimum condition obtained from response surface plots was concentration of nitric acid of 4.0 M,  $\text{W}/\text{PO}_4^{3-}$  weight ratio of 1.5:1 and leaching temperature of 90 °C. The maximum predicted value of percent recovery of tungsten oxide was 80.2%. From response surface plots, at the optimum condition the percent recovery of tungsten oxide increased by 31.8% from the predicted values. The results are shown in Table 3.3.

**Table 3.3** Comparison between predicted value of percent recovery of tungsten oxide and actual value of percent recovery of tungsten oxide

Experiment	Replications	% recovery	Average % recovery	Predicted values
RSM-1	1	113.5	112.0	80.2
	2	111.8		
	3	110.7		

### 3.2 Effect of Leaching Time

The experiments were carried out to investigate effect of leaching times under condition of 4.0 M of nitric acid, W/PO<sub>4</sub><sup>3-</sup> weight ratio of 1.5:1, leaching temperature of 90 °C, calcination temperature of 600 °C and calcination time for 30 minutes. The leaching times were varied in the range of 90-150 minutes. The effects of leaching times on percent recovery of tungsten oxide are shown in Table 3.4 and Figure 3.2. As presented in Table 3.4 and Figure 3.2, 108.2% of tungsten oxide was leached in 120 minutes. However, increasing leaching time from 120 to 150 minutes was not necessary because the recovery of tungsten virtually the same. From experiments it was clearly seen that 120 minutes of leaching time was enough for leaching tungsten from scheelite concentrates.

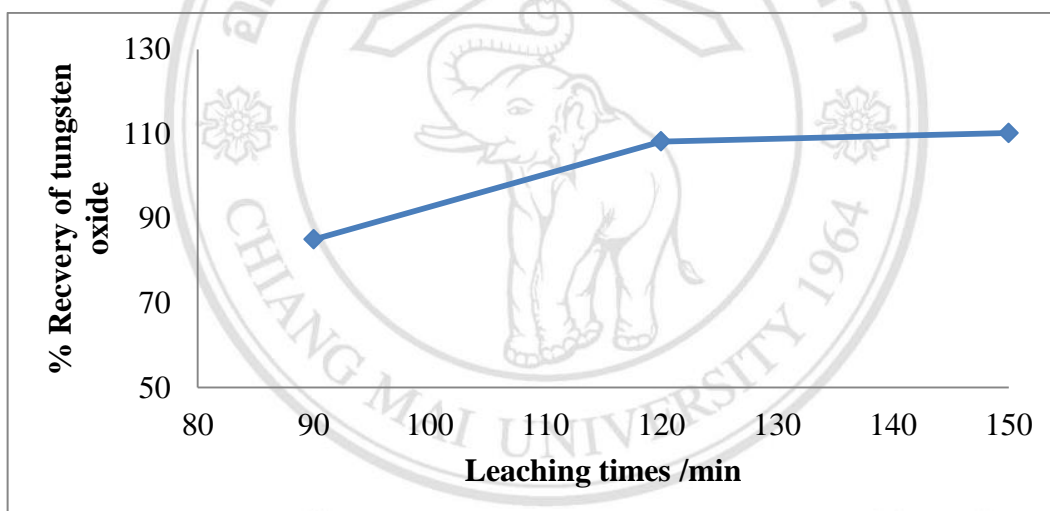


**Figure 3.2** Effects of leaching time on percent recovery of tungsten oxide.

Copyright© by Chiang Mai University  
All rights reserved

**Table 3.4** Effects of leaching times on weight, color and percent recovery of tungsten oxide

Experiments	Leaching time (min)	Replications	Sample weight (g)	Tungsten oxide weight (g)	Color	% Recovery	Average % recovery
RSM-2	90	1	2.0792	1.3704	Yellow	85.6	85.0±3.1
		2	2.0109	1.3590	Yellow	87.8	
		3	2.0216	1.2718	Yellow	81.7	
RSM-3	120	1	2.1280	1.8068	Yellow	110.3	108.2±4.9
		2	2.1820	1.7254	Yellow	102.7	
		3	2.0420	1.7686	Yellow	111.8	
RSM-4	150	1	2.0146	1.7432	Yellow	112.4	110.2±3.4
		2	2.0032	1.6396	Yellow	106.3	
		3	2.0998	1.8111	Yellow	112.0	

### 3.3 Effect of Calcination Temperature

The experiments were carried out to study effect of calcination temperature under condition of concentration of 4.0 M nitric acid, W/PO<sub>4</sub><sup>3-</sup> weight ratio of 1.5:1, leaching temperature of 90°C, leaching time for 120 minutes and calcination time for 30 minutes. The calcination temperatures were varied in the range of 500-800 °C. The effects of calcination temperatures on percent recovery of tungsten oxide are shown in Table 3.5 and Figure 3.3. As presented in Table 3.5 and Figure 3.3, percent recovery of tungsten oxide is practically independent of calcination temperature because amount of tungsten oxide depends on leaching process of tungsten. However, calcination temperatures affect the phase transformation and crystalline size.

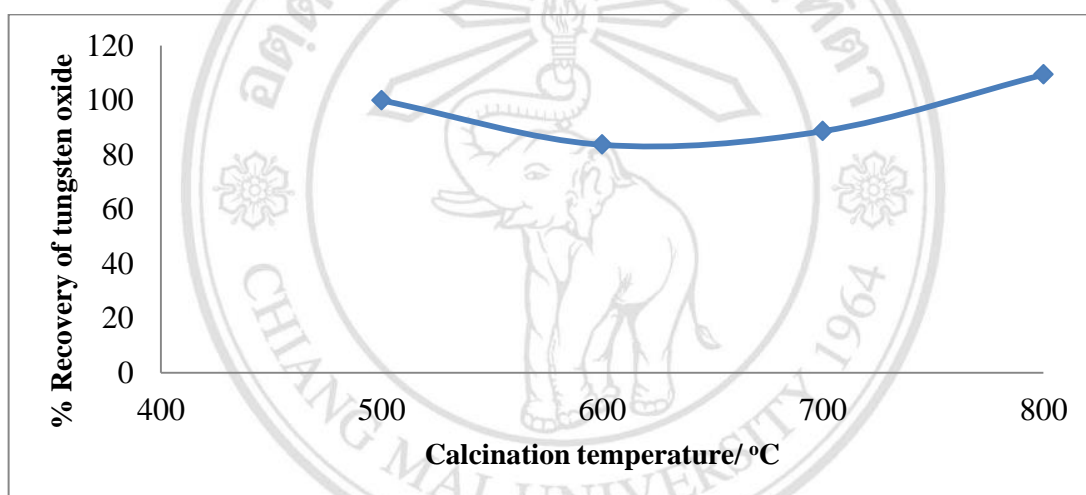


**Figure 3.3** Effects of calcination temperature on percent recovery of tungsten oxide.

ลิขสิทธิ์มหาวิทยาลัยเชียงใหม่  
Copyright© by Chiang Mai University  
All rights reserved

**Table 3.5** Effect of calcination temperature on weight, color and percent recovery of tungsten oxide

Experiments	Calcination temperature (°C)	Replications	Sample weight (g)	Tungsten oxide weight (g)	Color	% Recovery	Average % recovery
RSM-5	500	1	2.1519	1.5796	Light yellow	95.3	99.9±3.9
		2	2.0042	1.5757	Light yellow	102.1	
		3	2.0173	1.5866	White	102.1	
RSM-6	600	1	2.0553	1.2624	Light green	79.8	83.6±9.0
		2	2.0608	1.4895	Light yellow	93.9	
		3	2.0798	1.2334	Light green	77.0	
RSM-7	700	1	2.0663	1.4572	Green	91.6	88.6±2.6
		2	2.1850	1.4641	Green	87.0	
		3	2.0122	1.3508	Green	87.2	
RSM-8	800	1	2.0676	1.5871	Green	99.7	109.3±8.6
		2	2.0328	1.8184	Green	116.2	
		3	2.0932	1.8066	Green	112.1	

The phase transformation and crystal size of tungsten oxide at various calcination temperature were analyzed by X-ray diffraction technique. The X-ray diffraction pattern of product that obtained from calcination temperature of 500 °C is given in Figure 3.2. As presented in Figure 3.2, X-ray diffraction pattern of product, which obtained from calcination temperature of 500 °C, was not correspond to the standard X-ray diffraction pattern of tungsten oxide. However, X-ray diffraction pattern of product that obtained from calcination temperature of 500 °C matched with standard X-ray diffraction pattern of tungstophosphoric acid by the JCPDS card No. 50-0304. Therefore, 500 °C of calcination temperature was not enough for transformation of tungstophosphoric acid to tungsten oxide. This result agreed very well with previous work by Sebahattin Gurmen and co-worker [4]. In previous work, tungsten compound could be transformed into a pure tungsten oxide by simple thermal break-down process carried out at temperature equal or greater than 600 °C.

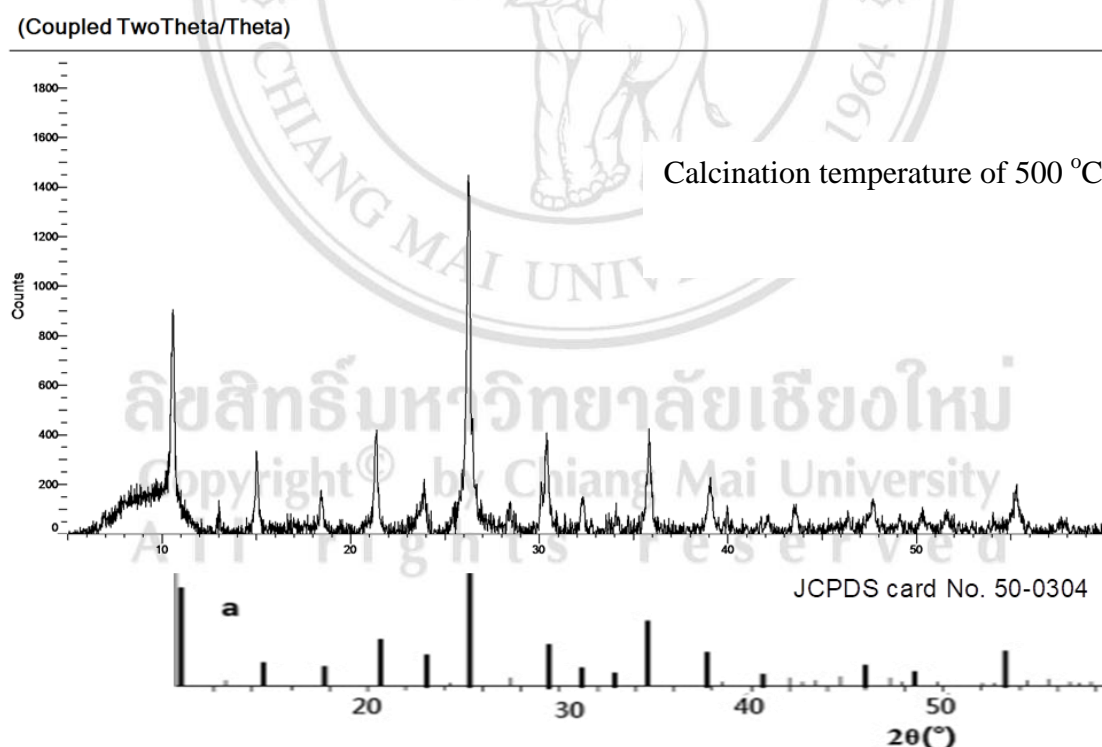


**Figure 3.4** The X-ray diffraction pattern of product obtained from calcination temperature of 500 °C and standard X-ray diffraction pattern of tungstophosphoric acid.

The X-ray diffraction patterns of products obtained from calcination temperatures of 600, 700 and 800 °C are given in Figure 3.3. As presented in Figure 3.3, X-ray diffraction patterns of products from calcination temperature of 600, 700 and 800°C matched with standard x-ray diffraction pattern of tungsten oxide by the JCPDS card No. 01-83-0950. The effect of calcination temperature on crystallite size was also shown by X-ray diffraction pattern in Figure 3.3. As presented in Figure 3.3, the X-ray diffraction peaks become sharper and narrower as the calcination temperature increases because the crystallinity and crystallite size increase at higher calcination temperature.

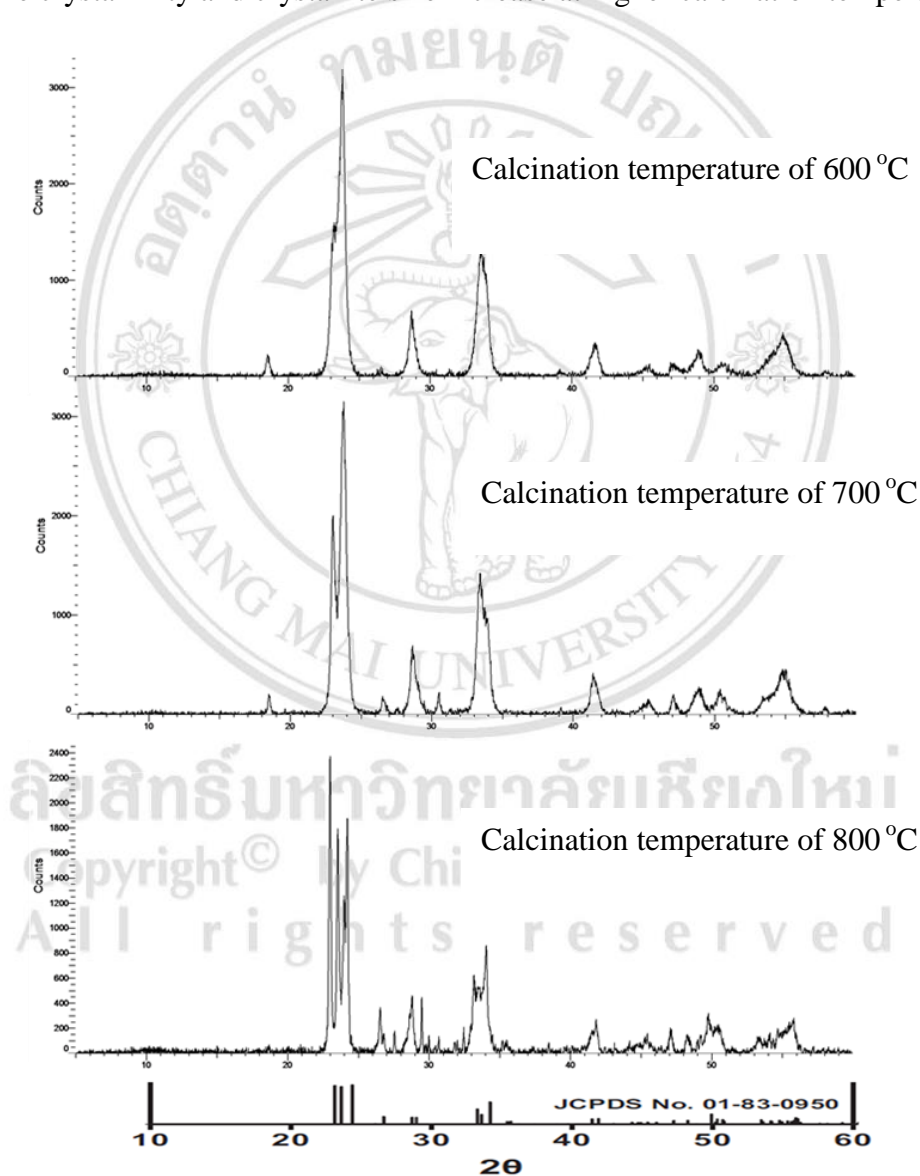


**Figure 3.5** The X-ray diffraction pattern of product obtained from calcination temperatures of 600, 700 and 800 °C and standard X-ray diffraction pattern of tungsten oxide



Furthermore, the crystallite size can be calculated from X-ray diffraction pattern using the Scherrer equation given by the equation 3.2.

$$\text{Particle size} = (0.94 \times \lambda) / (d \times \cos\theta) \quad (3.2)$$

where:  $\lambda = 1.54060 \text{ \AA}$  (in case of Cu- $\alpha$ )

$d$  = the full width at half maximum intensity of the peak in Rad

$$\theta = 2\theta/2$$

The crystallite size of tungsten oxide with different calcination temperature is shown in Table 3.6. As presented in Table 3.6, the size of tungsten oxide crystallites increases from 14.63 to 84.72 nm when the calcination temperature is raised from 600°C to 800 °C [74].

**Table 3.6** The crystallite size of tungsten oxide with different calcination temperature

Calcination temperature (°C)	Crystallite size (nm)
600	14.63
700	19.33
800	84.72

Increasing of the crystallite size with calcination temperature is related to the crystal growth. At high calcination temperature, the crystallite size increases because the grain boundary was removed [75]. However, energy cost saving is important in the commercial industries. Hence, calcination temperature of 600 °C was considered as the optimum temperature used in this work.

### 3.4 Effect of Calcination Time

Effect of calcination time on percent recovery of tungsten oxide was investigated under conditions of 4.0 M nitric acid, W/PO<sub>4</sub><sup>3-</sup> weight ratio of 1.5:1, leaching temperature of 90 °C, leaching time for 120 minutes and calcination temperature of 600 °C. The calcination times were varied in the range from 30-60 minutes. The effects of calcination time on percent recovery of tungsten oxide are shown in Table 3.7 and Figure 3.6. As presented in Table 3.7 and Figure 3.6, the recovery of tungsten oxide remained unchanged when the calcination times increased.

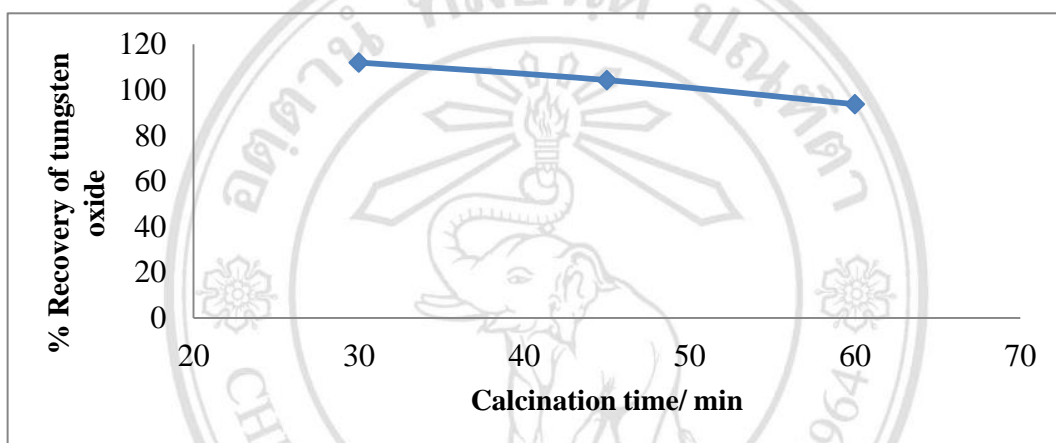


**Figure 3.6** Effects of calcination time on percent recovery of tungsten oxide.

**Table 3.7** Effect of calcination times on weight, color and percent recovery of tungsten oxide

Experiments	Calcination time (min)	Replications	Sample weight (g)	Tungsten oxide weight (g)	Color	% Recovery	Average % recovery
RSM-9	30	1	2.0270	1.7709	Yellow	113.5	112.0±1.4
		2	2.0294	1.7468	Yellow	111.8	
		3	2.0173	1.7192	Yellow	110.7	
RSM-10	45	1	2.0236	1.6802	Light green	107.8	104.3±7.9
		2	2.0336	1.4911	Light green	95.2	
		3	2.0441	1.7282	Light green	109.8	
RSM-11	60	1	2.0265	1.6280	Light green	104.3	93.7±11.1
		2	2.0107	1.4654	Light green	94.7	
		3	2.0160	1.2753	Light green	82.2	

The X-ray diffraction patterns of product, which obtained from calcination time of 30, 45 and 60 minutes are given in Figure 3.4. As shown in Figure 3.4, all of X-ray diffraction patterns of product match with standard X-ray diffraction pattern of tungsten oxide by JCPDS number 01-83-0950. The crystallite size of tungsten oxide with different calcination time are shown in Table 3.8. The result presented in Table 3.8 reveals that the crystallite size of tungsten oxide slightly increases with increase of calcination time. Therefore, 30 minutes of calcination time was chosen for this work.

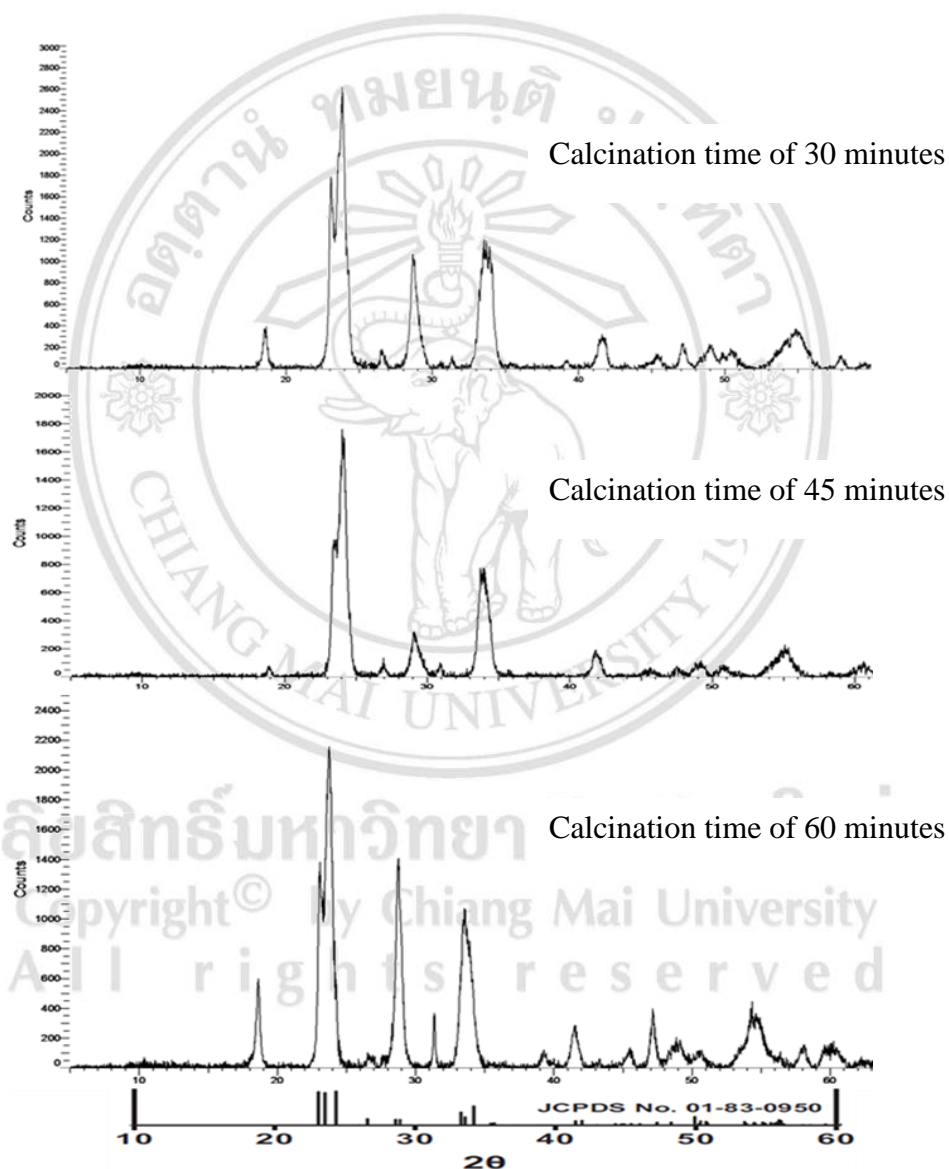


**Figure 3.7** The X-ray diffraction pattern of tungsten oxide that obtained from calcination time of 30, 45 and 60 minutes and standard X-ray diffraction pattern of tungsten oxide

**Table 3.8** The crystallite size of tungsten oxide with different calcination time

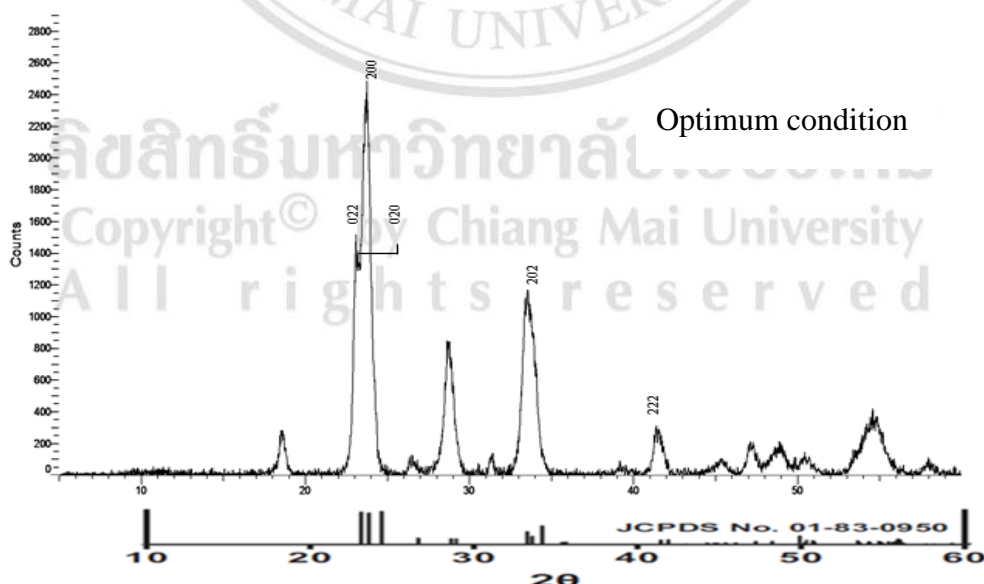
Calcination time (min)	Crystallite size (nm)
30	10.62
45	11.63
60	12.67

### 3.5 Characterization

The optimum condition for preparation of tungsten oxide based on aforementioned experiments as followed: 4.0 M nitric acid, W/PO<sub>4</sub><sup>3-</sup> weight ratio of 1.5:1, leaching temperature of 90 °C, leaching time for 120 minutes, calcination temperature of 600°C and calcination time for 30 minutes. The tungsten oxide, which was prepared under optimum condition, was characterized by the following methods.

#### 3.5.1 X-Ray Diffraction Spectroscopy (XRD)

The X-ray diffraction pattern of tungsten oxide that was prepared under optimum condition was given in Figure 3.5. As presented in Figure 3.5, the main characteristic peaks of product correspond to (022), (020), (200), (202) and (222) [76,-77]. These characteristic peaks match with the standard X-ray diffraction pattern of tungsten oxide by JCPDS card number 01-83-0950.

**Figure 3.8** The X-ray diffraction pattern of tungsten oxide that was prepared under optimum condition and standard X-ray diffraction pattern of tungsten oxide.

### 3.5.2 Fourier Transform Infrared Spectroscopy (FTIR)

The result which obtained from X-ray diffraction pattern, was confirmed by infrared absorption spectrum. Infrared absorption spectrum of tungsten oxide that obtained by preparation under optimum condition is shown in Figure 3.6. As presented in Figure 3.6, the infrared absorption spectrum of tungsten oxide presented a band at  $3446\text{ cm}^{-1}$ , sharp peak at  $1637\text{ cm}^{-1}$  and band at  $812\text{ cm}^{-1}$ . The band at  $3446\text{ cm}^{-1}$  corresponds to the symmetric stretching vibrations and intercalated water molecules ( $\text{W-OH}\dots\text{H}_2\text{O}$ ). The peak at  $1637\text{ cm}^{-1}$  corresponds to the bending vibration mode of absorbed water ( $\text{WO}\dots\text{OH}$ ) ( $\text{W}\dots\text{OH}$ ). The peak at  $1637\text{ cm}^{-1}$  was produced by moisture contamination. The band at  $812\text{ cm}^{-1}$  is assigned to be the stretching vibration mode of the bridging oxygen atoms ( $\text{O-W-O}$ ). Thus, this infrared absorption spectrum corresponded the tungsten oxide [78].

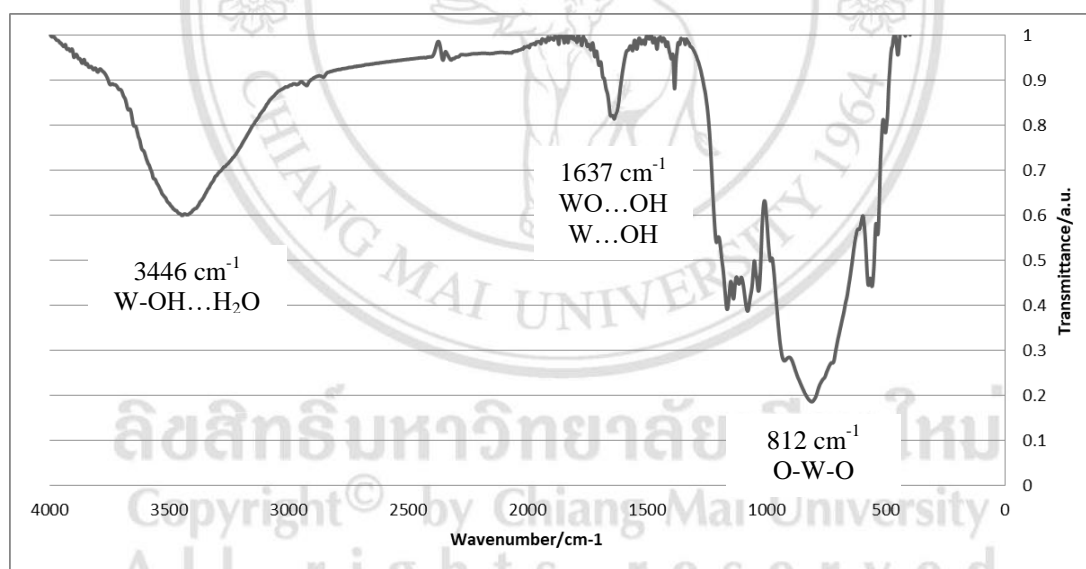


**Figure 3.9** FTIR spectrum of tungsten oxide obtained by preparation under optimum condition.

### 3.5.3 Scanning Electron Microscopy (SEM) Equipped with Energy-Dispersive X-ray Spectroscopy (EDX)

The surface morphology and composition of the tungsten oxide that obtained by preparation under optimum condition was investigated by Scanning Electron Microscopy (SEM) equipped with Energy Dispersive X-ray Spectroscopy (EDX). Figure 3.7 shows the SEM image of tungsten oxide that obtained by preparation under optimum condition (A) and the SEM image of tungsten oxide from previous report (B). Figure 3.7 (A) indicates that the tungsten oxide that obtained from preparation under optimum condition showed the formation of particles of irregular shapes. Furthermore, the SEM image of tungsten oxide that obtained from preparation under optimum condition showed a good agreement with previous work that reported by Sebastian Germen and co-worker [79].

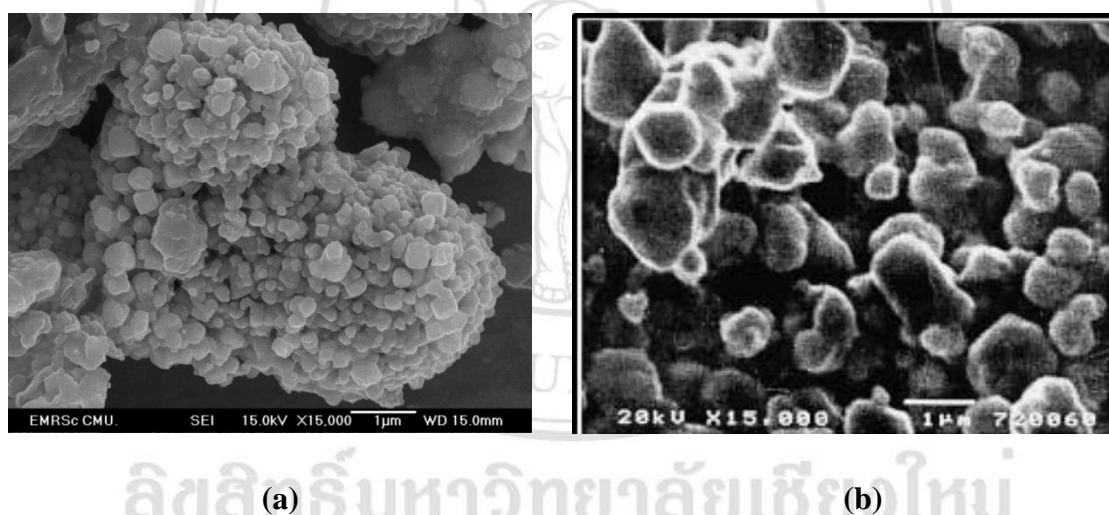


**Figure 3.10** (a) Micrograph of the tungsten oxide obtained by preparation under optimum condition and (b) micrograph of tungsten oxide [78].

The chemical composition of the particle of tungsten oxide that was prepared under optimum condition was analyzed by energy dispersive X-ray spectroscopy. The EDX pattern of tungsten oxide that was prepared under optimum condition is shown in Figure 3.8. As presented in Figure 3.8, this EDX pattern shows tungsten and oxygen as major elements in the product. Furthermore, the EDX microanalysis indicated that slight amount of phosphorus and calcium in the product. The phosphorus signal related to the

phosphate anion, which was used as the chelating agent for leaching tungsten from scheelite concentrate. The calcium signals relate to the scheelite concentrate ( $\text{CaWO}_4$ ) sample. This result illustrate that, phosphorus and calcium lead to get percent recovery greater than 100%. Therefore, the tungsten oxide can be prepared from Samoeng's scheelite concentrate by this developed method.

Element	Weight%	Atomic%
O	17.11	67.75
W	77.19	24.61
Ca	3.57	4.31
P	2.13	3.33
Totals	100.00	

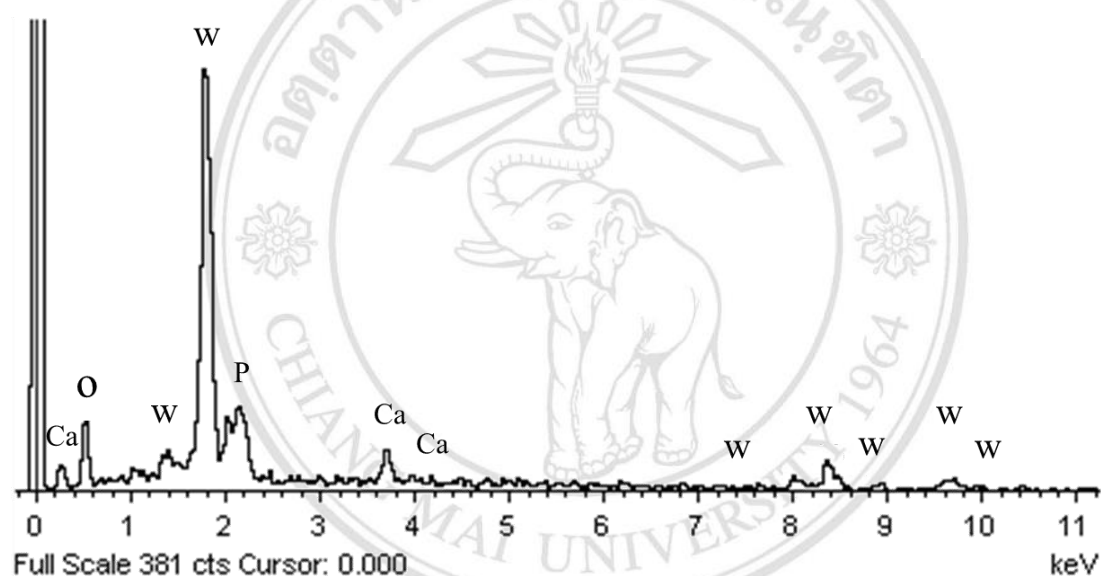


**Figure 3.11** EDX elemental microanalysis analysis of tungsten oxide that was prepared under optimum condition.



## CHAPTER 4

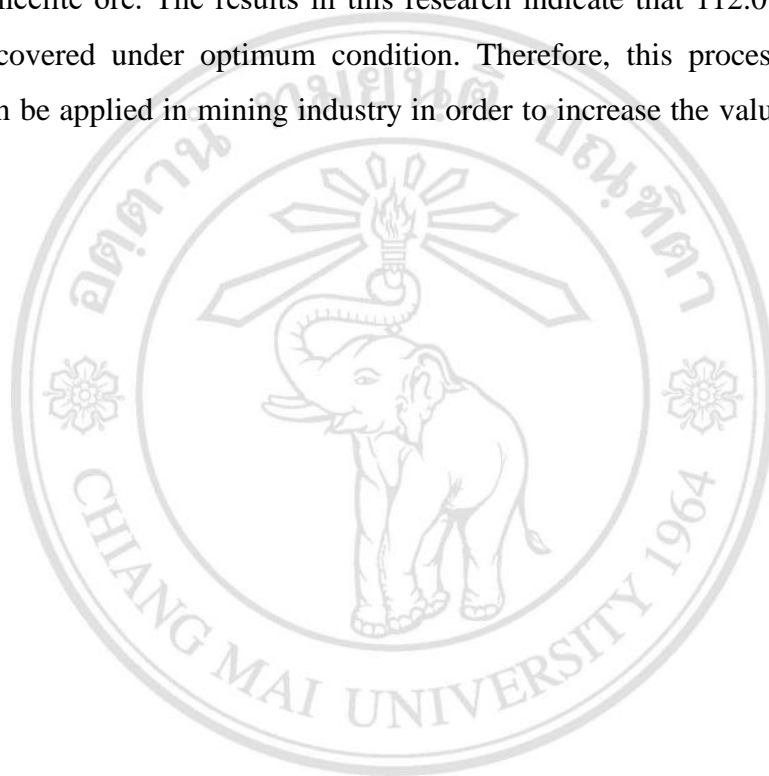
### Conclusions

Tungsten oxide is chemical compound consist of transition metal tungsten and oxygen. This chemical compound is widely used in metal industry such as used to manufacture tungstate for X-ray screen phosphor and fire proofing fabrics. At present, Bo Kaeo mine in Samoeng District, Chiang Mai exports tungsten in the form of scheelite concentrate. In order to increase the value of export of tungsten, the process for preparation of tungsten oxide from Samoeng's scheelite ore was studied. Chemical compositions in Samoeng's scheelite concentrate was investigated by X-ray fluorescence spectrometer. The results indicated that Samoeng's scheelite concentrate contained 77% of tungsten oxide.

The leaching of tungsten from scheelite using nitric acid and phosphoric acid as chelating agent has been chosen for a part of this work because this method is simple, not require high temperature and low waste generation. Various parameters namely, concentration of  $\text{HNO}_3$ , leaching temperature, leaching time,  $\text{W}/\text{PO}_4^{3-}$  weight ratio, calcination temperature and calcination time were studied for optimum condition. However, three important parameters, which affected the recovery of tungsten including concentration of  $\text{HNO}_3$ , leaching temperature and  $\text{W}/\text{PO}_4^{3-}$  weight ratio, were chosen to study first by applying central composite design to model the experiment. The result was indicated in form of response surface plots using response surface methodology (RSM). The optimum leaching condition that obtained from response surface plots was 4.0 M nitric acid,  $\text{W}/\text{PO}_4^{3-}$  weight ratio of 1.5:1 and leaching temperature of 90 °C. At the optimum leaching condition that obtained from response surface plots, the maximum predicted value of percent recovery of tungsten oxide was 80.2%. However, the preparation of tungsten oxide was carried out under the optimum leaching condition and it was found that the percent recovery of tungsten oxide was greater than the

predicted value of 31.8%. The optimum leaching condition, which obtained from response surface plots, was chosen to investigate the effect of leaching time, calcination temperature, calcination time on recovery of tungsten oxide. The results indicated that, the optimum leaching time, optimum calcination time and optimum calcination temperature were 120 minutes, 30 minutes and 600 °C, respectively.

This research developed the effective process for preparing tungsten oxide from Samoeng's scheelite ore. The results in this research indicate that 112.0% of tungsten oxide was recovered under optimum condition. Therefore, this process, which was developed, can be applied in mining industry in order to increase the value of export of tungsten.



ลิขสิทธิ์มหาวิทยาลัยเชียงใหม่  
Copyright© by Chiang Mai University  
All rights reserved

## REFERENCES

- [1] The Institute for the Promotion of Teaching Science and Technology (IPST), Tin Mine in Ban Bo Kaeo. [online]. Available at: [http://fieldtrip.ipst.ac.th/intro\\_sub\\_content.php?content\\_id=4&content\\_folder\\_id=57](http://fieldtrip.ipst.ac.th/intro_sub_content.php?content_id=4&content_folder_id=57) (Accessed: 3<sup>rd</sup> March 2016).
- [2] D. Mari, L. Llanes, C. E. Nebel, Comprehensive Hard Materials, New York: Elsevier Ltd., 2014.
- [3] E. Lassner, W. Schubert, Tungsten: Properties, Chemistry, Technology of the Element, Alloys, and Chemical Compounds, New York: Kluwer Academic/Plenum, 1999.
- [4] S. Gurmen, G. Orhan, S. Timur, Jahrgang, 2003, 57: 722-726.
- [5] W. Zhang, J. Li, Z. Zhao, International Journal of Refractory Metal and Hard Materials, 2015, 52: 78-84.
- [6] F. Bendebane, F. Ismail, L. Bouziane, Energy Procedia, 2014, 50: 642 – 651.
- [7] Agency for Toxic Substances and Disease Registry (ATSDR), Addendum to the Toxicological Profile for Tungsten, Atlanta: Division of Toxicology and Human Health Sciences, 2015.
- [8] M. C. Rao, Journal of Non-Oxide Glasses, 2013, 5: 1-8.
- [9] N.N. Greenwood, A. Earnshaw, Chemistry of the Elements, Oxford: Pergamon Press, 1985.
- [10] R. Tilley, Colour and the Optical Properties of Materials, 2<sup>nd</sup> ed., Hoboken, New Jersey: John Wiley & Sons Inc., 20.

- [11] Teledyne Leeman Labs, Analysis of Trace Elements in Tungsten Trioxide Using the Prodigy DC Arc Spectrometer, Hudson, 2014.
- [12] University of Cambridge,  $\text{WO}_3$  - Tungsten (VI) Trioxide, [online]. Available at: <https://ascg.msm.cam.ac.uk/materials/wo3.php> (Accessed: 10<sup>th</sup> December 2017).
- [13] O. Pokakornvijarn, Ore, Bangkok: Geology Division/Department of Mineral Resources, 2000.
- [14] J. W. Anthony, R. A. Bideaux, K. W. Bladn, M.C. Nicholas, Handbook of Mineralogy, Tucson Arizona: Mineral Data Publishing, 1990.
- [15] Online Database of Luminescent minerals, [online]. Available at: <https://www.fluomin.org/uk/fiche.php?id=202> (Accessed: 9<sup>th</sup> December 2017).
- [16] A.R. Burkin, Chemical Hydrometallurgy; Theory and Principle, Singapore: World Scientific Publishing Co. Pte. Ltd., 2001.
- [17] T. Rosenqvist, Principle of Extractive Metallurgy, New York: McGraw-Hill Inc., 1974.
- [18] J. J. Moore, Chemical Metallurgy, 2<sup>nd</sup> ed., Oxford: Butterworth-Heinemann Ltd., 1990.
- [19] A. Vignes, Extractive Metallurgy 3: Processing Operations and Routes, London: ISTE Ltd., 2011.
- [20] D. Reid, Leaching : Definition & Process [online]. Available at: <https://study.com/academy/lesson/leaching-definition-process.html> (Accessed: 24<sup>th</sup> August 2018).
- [21] S. Murmson, Describe the Process of Electrolysis in the Production of Metals [online]. Available at: <https://education.seattlepi.com/describe-process-electrolysis-production-metals-4411.html> (Accessed: 24<sup>th</sup> August 2018).
- [22] M.B. Kirkham, Principles of Soil and Plant Water Relations, 2<sup>nd</sup> ed., New York: Elsevier Academic Press, 2014.

- [23] C. P. O'Donnell, C. Fagan, P. J. Cullen, Process Analytical Technology for the Food Industry, New York: Springer Science & Business Media, 2014.
- [24] K. Leiviska, Introduction to Experiment Design, Oulu: University of Oulu, 2013.
- [25] M. Cavazzuti, Design of Experiment, Optimization Methods from Theory to Design Scientific and Technological Aspects in Mechanics, New York: Springer Science & Business Media, 2012.
- [26] G. Hanrahan, K. Lu, Critical Reviews in Analytical Chemistry, 2006, 36: 141-151.
- [27] R. G. Brereton, Chemometric: Data Analysis for the Laboratory and Chemical Plant, West Sussex: John Wiley & Sons Ltd., 2007: 76-84.
- [28] R. G. Brereton, Applied Chemometric for Scientists, West Sussex: John Wiley & Sons Ltd., 2007.
- [29] H. Hentzner, C. Schmid, S. Tremmel, K. Dust, S. Wartzack, Coatings, 2014, 4: 772-795.
- [30] Math Works, Response Surface Designs, [online]. Available at: <https://www.mathworks.com/help/stats/response-surface-designs.html> (Accessed: 4<sup>th</sup> December 2017).
- [31] M. Tranmer, M. Elliot, Multiple Linear Regression: Cathie Marsh Center of Census and Survey Research, 2008, [online]. Available at: [hummedia.Manchester.ac.uk/institutes/.../2008-19-multiple-linear-regression.pdf](http://hummedia.Manchester.ac.uk/institutes/.../2008-19-multiple-linear-regression.pdf) (Accessed: 7<sup>th</sup> September 2018).
- [32] K. A. Marill, Academic Emergency Medicine, 2004, 11: 94-102.
- [33] M. Bremer, Multiple Linear Regression, [online]. Available at: <http://mezeylab.cb.bscb.cornell.edu/labmembers/documents/supplement%20-%20multiple%20regression.pdf> (Accessed: 7<sup>th</sup> September 2018).
- [34] N. E. Helwig, Multiple Linear Regression, [online]. Available at: [users.stat.umn.edu/~helwig/notes/mlr-Notes.pdf](http://users.stat.umn.edu/~helwig/notes/mlr-Notes.pdf) (Accessed: 7<sup>th</sup> September 2018).

- [35] M. A. Bezerra, R. E. Santell, E. P. Oliveira, L. S. Villar, L. A. Escateira, *Talanta*, 2008, 76: 965-979.
- [36] A. I. Khuri, S. Mukhopadhyay, *WIREs Computation AI Statistics*, 2010, 2: 128-149.
- [37] T. Butterfield, Method of Steepest Ascent, [online]. Available at: [https://www.che.utah.edu/~tony/course/material/ExperimentalDesign/30\\_meth\\_of\\_steep\\_asc.php](https://www.che.utah.edu/~tony/course/material/ExperimentalDesign/30_meth_of_steep_asc.php) (Accessed: 7<sup>th</sup> September 2018).
- [38] D. A. Skoog, F.J. Holler, R. Crouch, *Principles of Instrumental Analysis*, 6<sup>th</sup> ed., Cole: Thomson Brooks, 2007.
- [39] G. W. Ewing, *Instrumental Methods of Chemical Analysis*, 4<sup>th</sup> ed., New York: McGraw-Hill Book Company, 1975.
- [40] C. Whiston, *X-ray method*, London: Thames Polytecnic, 1987.
- [41] BRUKER, X-ray Diffraction and Elemental Analysis, [online]. Available at: <https://www.bruker.com/products/x-ray-diffraction-and-elemental-analysis/handheld-xrf/how-xrf-works.html> (Accessed: 28<sup>th</sup> September 2017).
- [42] R. D. Braun, *Introduction to Instrumental Analysis*, Singapore: McGraw-Hill Book Company, 1987.
- [43] J. A. Wolska, B. A. R. Vrebo, XRF: A Powerful Oil Analysis Tool, [online] Available at: <http://www.machinerylubrication.com/Read/602/xrf-oil-analysis> (Accessed: 2<sup>nd</sup> October 2017).
- [44] E. Pungor, *A Practical Guide to Instrumental Analysis*, Florida: CRC Press, 2000.
- [45] H. H. Willard, L. L. Merritt, J. A. Dean, F. A. Settle, *Instrumental methods of analysis*, California: Wadsworth publishing company, 1988.
- [46] B. L. Dutrow, C.M. Clark, X-ray Powder Diffraction (XRD), [online]. Available at: [https://serc.carleton.edu/research\\_education/geochemsheets/techniques/XRD.html](https://serc.carleton.edu/research_education/geochemsheets/techniques/XRD.html) (Accessed: 15<sup>th</sup> October 2017).

- [47] B. F. Pease, Basic Instrumental Analysis, New York: D. Van Nostrand Company, 1980.
- [48] D. Henry, N. Eby, J. Goodge, D. Mogk, X-ray reflection in accordance with Bragg's Law, [online] Available at: [https://serc.carleton.edu/research\\_education/geochemsheets/BraggsLaw.html](https://serc.carleton.edu/research_education/geochemsheets/BraggsLaw.html) (Accessed: 21<sup>st</sup> November 2017).
- [49] M. F. Peyronel, A. G. Marangoni, X-Ray Powder Diffractometry, [online]. Available at: <http://lipidlibrary.aocs.org/Biochemistry/content.cfm?ItemNumber=40299> (Accessed: 6<sup>th</sup> August 2018).
- [50] Thermo Nicolet Co, Introduction to Fourier Transform Infrared Spectrometry, [online]. Available at: [https://www.niu.edu/analyticallab/\\_pdf/ftir/FTIRintro.pdf](https://www.niu.edu/analyticallab/_pdf/ftir/FTIRintro.pdf) (Accessed: 18<sup>th</sup> January 2018).
- [51] A. Tiwari, J. Rawlins, L. H. Hihara, Intelligent Coatings for Corrosion Control, Oxford: Elsevier Inc., 2015.
- [52] A. Ravindran, Electromagnetic Spectrum Diagram, [online]. Available at: <https://myasadata.larc.nasa.gov/science-practices/electromagnetic-diagram/> (Accessed: 6<sup>th</sup> August 2018).
- [53] D. L. Pavia, G. M. Lampman, G. S. Kriz, J. R. Vyvyan, Introduction to Spectroscopy, 4<sup>th</sup> ed., California: Brooks, 2009.
- [54] Chemistry Libretexts, Fourier Transform Infrared Spectroscopy (FTIR), [online]. Available at: [https://chem.libretexts.org/LibreTexts/Howard\\_University/Howard%3A\\_Physical\\_Chemistry\\_Laboratory/14.\\_Fourier\\_Transform\\_Infrared\\_Spectroscopy\\_\(FTIR\)](https://chem.libretexts.org/LibreTexts/Howard_University/Howard%3A_Physical_Chemistry_Laboratory/14._Fourier_Transform_Infrared_Spectroscopy_(FTIR)) (Accessed: 18th January 2018).
- [55] B.C. Smith, Fundamentals of Fourier Transform Infrared Spectroscopy, 2<sup>nd</sup> ed., New York: CRC press, 2011: 19-49.
- [56] S. Swapp, Scanning Electron Microscopy (SEM), [online]. Available at: [https://serc.carleton.edu/research\\_education/geochemsheets/techniques/SEM.html](https://serc.carleton.edu/research_education/geochemsheets/techniques/SEM.html) (Accessed: 20<sup>th</sup> October 2017).

- [57] S. R. Shamsudin, Scanning Electron Microscope (SEM) & How It Works, [online]. Available at: <http://emicroscope.blogspot.com/2011/03/scanning-electron-microscope-sem-how-it.html> (Accessed: 17<sup>th</sup> October 2017).
- [58] W. Zhou, Z. L. Wang, Scanning Microscopy for Nanotechnology: Techniques and Applications, New York: Springer Science + Business Media, LLC, 2007: 1-39.
- [59] Research Group Electronchemical and Surface Engineering, Vrije Universiteit Brussel, [online]. Available at: <https://www.surfgroup.be/semidx> (Accessed: 26<sup>th</sup> October 2017).
- [60] Energy Dispersive Spectroscopy, 2<sup>nd</sup> ed., West Sussex: John Wiley & Sons Ltd, 2015.
- [61] Central Facility for Advanced Microscopy and Microanalysis, Introduction to Energy Dispersive X-ray Spectroscopy (EDS) [online]. Available at: <https://cfamm.ucr.edu/documents/eds-intro.pdf> (Accessed: 11<sup>th</sup> September 2018).
- [62] J. Goodge, Energy Dispersive X-Ray Spectroscopy (EDS) [online]. Available at: [https://serc.carleton.edu/research\\_education/geochemsheets/eds.html](https://serc.carleton.edu/research_education/geochemsheets/eds.html) (Accessed: 11<sup>th</sup> September 2018).
- [63] G. D. Christian, Analytical Chemistry, 4<sup>th</sup> ed., New York: John Wiley & Sons Inc., 1986.
- [64] D. A. Skoog, D. M. West, F. J. Holler, S. R. Crouch, Analytical Chemistry An Introduction, New York: Thomson Learning, 2000.
- [65] D. A. Skoog, D. M. West, F. J. Holler, S. R. Crouch, Fundamentals of Analytical Chemistry, 9<sup>th</sup> ed., Singapore: Cengage Learning Asia Pte. Ltd., 2014.
- [66] D. J. Pietrzyk, C. W. Frank, Analytical Chemistry an Introduction, New York: Academic Press Inc., 1974: 221-222.
- [67] J. I. Martins, Mineral Processing and Extraxtive Matallurgy Review, 2014, 35: 23-49.



- [68] Z. Zhao, J. Li, S. Wang, H. Li, M. Liu, P. Sun, Y. Li, *Hydrometallurgy*, 2011, 108:152-156.
- [69] Z. Zhao, Y. Liang, X. Liu, A. Chen, H. Li, *International Journal of Refractory Metal and Hard Materials*, 2011, 29: 739-742.
- [70] K. Srinivas, T. Sreenivas, R. Natarajan, N.P.H. Padmanabham, *Hydrometallurgy*, 2000, 58: 43-50.
- [71] H.G. Li, *Transactions of Nonferrous Metals Society of China*, 2004, 14: 366-369.
- [72] Y. Wang, S. Yang, H. Li, *International Journal of Refractory Metal and Hard Materials*, 2016, 54: 284-288.
- [73] S. Gurmen, S. Timur, C. Arslan, I. Duman, *Hydrometallurgy*, 1999, 51: 227-238.
- [74] C. G. Kumar, S. Pombala, Y. Poornachandra, S.V. Agarwal, *Nanobiomaterials in Antimicrobial Therapy*, 2016, 6: 103-152.
- [75] P. M. Shafi, A. C. Bose, Impact of crystalline defects and size on X-ray line broadening: A phenomenological approach for tetragonal SnO<sub>2</sub> nanocrystals [online]. Available at: <https://aip.scitation.org/doi/full/10.1063/1.4921452> (Accessed: 11<sup>th</sup> July 2018).
- [76] O. Nimittrakoolchai, S. Supothina, Synthesis and characterization of tungsten oxide (WO<sub>3</sub>) nanoplate [online]. Available at: [www2.mtec.or.th/th/seminar/msativ/pdf/CP17.pdf](http://www2.mtec.or.th/th/seminar/msativ/pdf/CP17.pdf) (Accessed: 11<sup>th</sup> July 2018).
- [77] C. Chacon, M. Rodriguez-Perez, G. Oskam, G. Rodriguez-Gattorno, *Journal of Materials Science: Materials in Electronics*, 2015, 26: 5526-5531.
- [78] O. Rezaee, H. M. Chenari, F. E. Ghodsi, *Journal of Sol-Gel Science and Technology*, 2016, 80: 109–118.
- [79] S. Gurmen, S. Timur, C. Arslan, I. Duman, *Scandinavian Journal of Metallurgy*, 2002, 31: 221-228.

## CURRICULUM VITAE

<b>Author's Name</b>	Ms. Methiyanun Suepkham
<b>Date / Year of Birth</b>	November 22, 1991
<b>Education</b>	Master of Science (Chemistry), Chiang Mai University, 2018 Bachelor of Science (Chemistry), Chiang Mai University, 2013
<b>Publication</b>	Methiyanun Suepkham and Sukjit Kungwankunakorn, Preparation of Tungsten Oxide from Scheelite Ores from Samoeng Distric, Chiang Mai Province. International Sciencetific Conference on Engineering and Applied Sciences, 27-29 June 2018, Okinawa, Japan



ลิขสิทธิ์มหาวิทยาลัยเชียงใหม่  
Copyright© by Chiang Mai University  
All rights reserved